Pre-monsoon air quality over Lumbini, a world heritage site along the Himalayan foothills

Dipesh Rupakheti[1,2*], Bhupesh Adhikary[3], Puppala Siva Praveen[3], Maheswar Rupakheti[4,5], Shichang Kang[6,7*], Khadak Singh Mahata[4], Manish Naja[8], Qianggong Zhang[1,7], Arnico Kumar Panday[3], Mark G. Lawrence[4]

[1]Key Laboratory of Tibetan Environment Changes and Land Surface Processes, Institute of Tibetan Plateau Research, Chinese Academy of Sciences, Beijing 100101, China
[2]University of Chinese Academy of Sciences, Beijing 100049, China
[3]International Centre for Integrated Mountain Development (ICIMOD), Kathmandu, Nepal
[4]Institute for Advanced Sustainability Studies (IASS), Potsdam 14467, Germany
[5]Himalayan Sustainability Institute (HIMSI), Kathmandu, Nepal
[6]State Key Laboratory of Cryospheric Science, Cold and Arid Regions Environmental and Engineering Research Institute (CAREERI), Lanzhou 730000, China
[7]Center for Excellence in Tibetan Plateau Earth Sciences, Chinese Academy of Sciences, Beijing 100085, China
[8]Aryabhatta Research Institute of Observational Sciences (ARIES), Nainital, India

Correspondence to:

Dipesh Rupakheti (dipesh.rupakheti@itpcas.ac.cn), Shichang Kang (shichang.kang@lzb.ac.cn)

Abstract

Lumbini, in southern Nepal, is a UNESCO world heritage site of universal value as the birthplace of Buddha. Poor air quality in Lumbini and surrounding regions is a great concern for public health as well as for preservation, protection and promotion of Buddhist heritage and culture. We present here results from measurements of ambient concentrations of key air pollutants (PM, BC, CO, O_3) in Lumbini, first of its kind for Lumbini, conducted during an intensive measurement period of three months (April-June 2013) in the pre-monsoon season. The measurements were carried out as a part of the international air pollution measurement campaign; SusKat-ABC (Sustainable Atmosphere for the Kathmandu Valley - Atmospheric Brown Clouds). The main objective of this work was to understand and document the level of air pollution, diurnal characteristics and the influence of open burning on air quality in Lumbini. The hourly average concentrations during the entire measurement campaign ranged as follows: BC: 0.3 - 30.0 μg m^{-3}, PM_1: 3.6-197.6 μg m^{-3}, $PM_{2.5}$: 6.1 - 272.2 μg m^{-3}, PM_{10}: 10.5 - 604.0 μg m^{-3}, O_3: 1.0 - 118.1 ppbv, and CO: 125.0 - 1430.0 ppbv. These levels are comparable to other very heavily polluted sites in South Asia. Higher fraction of coarse mode PM was found as compared to other nearby sites in the Indo-Gangetic Plain region. ΔBC/ΔCO ratio obtained in Lumbini indicated considerable contributions of emissions from both domestic and transportation sectors. The 24-h average $PM_{2.5}$ and PM_{10} concentrations exceeded the WHO guideline very frequently (94% and 85% of the sampled period, respectively), which implies significant health risks for the residents and visitors in the region. These air pollutants exhibited clear diurnal cycles with high values in the morning and evening. During the study period, the worst air pollution episodes were mainly due to agro-residue burning and regional forest fires combined with meteorological conditions conducive of pollution transport to Lumbini. Fossil fuel combustion also contributed significantly, accounting for more than half of the ambient BC concentration according to aerosol spectral light absorption coefficients obtained in Lumbini. WRF-STEM, a regional chemical transport model, was used to simulate the meteorology and the concentrations of pollutants to understand the pollutant transport pathways. The model estimated values were ~ 1.5 to 5 times lower than the observed concentrations for CO and PM_{10} respectively. Model simulated regionally tagged CO tracers showed that the majority of CO came from the upwind region of Ganges Valley. Model performance needs significant

improvement in simulating aerosols in the region. Given the high air pollution level, there is a clear and urgent need for setting up a network of long-term air quality monitoring stations in the greater Lumbini region.

1. **Introduction**

The Indo-Gangetic plain (IGP) stretches over 2000 km encompassing a vast area of land in northern South Asia: the eastern parts of Pakistan, most of northern and eastern India, southern part of Nepal, and almost all of Bangladesh. The Himalayan mountains and their foothills stretch along the northern edge of IGP. The IGP region is among the most fertile and most intensely farmed region of the world. It is a heavily populated region with about 900 million residents or 12% of the world's population. Four megacities - Lahore, Delhi, Kolkata, and Dhaka are located in the IGP region, with dozens more cities with populations exceeding one million. The region has witnessed impressive economic growth in recent decades but unfortunately it has also become one of the most polluted, and an air pollution 'hot spot' of local, regional and global concern (Ramanathan et al., 2007). Main factors contributing to air pollution in the IGP and surrounding regions include emissions from vehicles, thermal power plants, industries, biomass and fossil fuel used in cooking and heating activities, agricultural activities, crop residue burning and forest fires. Air pollution gets transported long distances away from emission sources and across national borders. As a result, the IGP and adjacent regions get shrouded with a dramatic annual buildup of regional scale plumes of air pollutants, known as Atmospheric Brown Clouds (ABC), during the long and dry winter and pre-monsoon seasons each year (Ramanathan and Carmichael, 2008). Figure 1 shows monthly synoptic wind and mean aerosol optical depth (AOD) during April-June, 2013 over South Asia. Very high aerosol optical depth along the entire stretch of IGP reflects severity of air pollution over large areas in the region.

Poor air quality continues to pose significant threat to human health in the region. In a new study of global burden of disease released recently, Forouzanfar et al. (2015) estimated that in 2013 around 1.7 million people died prematurely in Pakistan, India, Nepal, and Bangladesh as a result of air pollution exposure, nearly 30% of global total premature deaths due to air pollution. Air pollution also affects precipitation (e.g. South Asian monsoon), agricultural productivity, ecosystems, tourism, climate, and broadly socio-economic and national development goals of the

80 countries in the region (Burney and Ramanathan, 2014; Shindell et al., 2012; Ramanathan and
81 Carmichael, 2008). It has also been linked to intensification of cold wave and winter fog in the
82 IGP region over recent decades (Lawrence and Lelieveld, 2010 and references therein; Safai et
83 al., 2009; Ganguly et al., 2006). Besides high levels of aerosol loading as shown in Fig. 1, Indo-
84 Gangetic plains also have very high levels of ground level ozone or tropospheric ozone (O_3)
85 (e.g., Ramanathan and Carmichael (2008)) which is a toxic pollutant to plant and human health,
86 and a major greenhouse gas (IPCC, 2013; Shindell et al., 2012; Mohnen et al., 1993). South
87 Asia, in particular IGP region, has been projected to be the most ozone polluted region in world
88 by 2030 (Stevenson et al., 2006). Majority of crop loss in different parts of the world results from
89 effects of ozone on crop health and productivity (Shindell et al., 2012). Burney and Ramanathan
90 (2014) also reported a significant loss in wheat and rice yields in India from 1980 to 2010 due to
91 direct effects of black carbon (BC) and ozone (O_3). BC and O_3 are two key short-lived climate
92 pollutants (SLCP). Similarly, species like fine particles and carbon monoxide (CO) are potent to
93 health damages by posing impacts upon the respiratory and cardiovascular system and even also
94 to the climate system (Singh et al., 2017 and references therein). Because of the IGP's close
95 proximity to the Himalaya-Tibetan plateau region, this once relatively clean region, is now
96 subjected to increasing air pollution transported from regions such as the IGP, which can exert
97 additional risks to sensitive ecosystems in the mountain region (e.g., (Lüthi et al., 2015;
98 Marinoni et al., 2013; Duchi et al., 2011). However, air pollution transport pathways to
99 Himalayas are still not yet fully understood.

100 Monuments and buildings made with stones are vulnerable to air pollution damage
101 (Brimblecombe, 2003; Gauri and Holdren, 1981). The damage to the monuments and buildings
102 could be in various forms like corrosion, soiling, abrasion and discoloration. For example, a
103 recent study has reported that deposition of light absorbing aerosol particles (black carbon,
104 brown carbon) and dust is responsible for the discoloration of Taj Mahal, a world famous
105 monument in India (Bergin et al., 2015). Lumbini, located near the northern edge of the central
106 Indo-Gangetic plain, is famous as the birthplace of the Lord Buddha and thus a UNESCO world
107 heritage site of outstanding universal value to humanity. Since the study area is renowned due to
108 its historical and archaeological significance, Lumbini is getting the worldwide attention also for

poor air quality in the region. There was no regular air quality monitoring in Lumbini at the time of our measurement campaign.

Through this study, we want to understand the level of air pollution, its diurnal characteristic, and the influence of open burning on air quality in Lumbini. We carried out continuous measurements of ambient concentrations of key air pollutants (PM, BC, CO, O_3) and meteorological parameters during an intensive measurement period of three months (April-June) in the year 2013. These are the first reported pollutant measurements for Lumbini. A regional chemical transport model called Sulfur Transport and dEposition Model (STEM) was used to simulate the variations of meteorological parameters and air pollutants during the observation period to examine the extent to which a state-of-the-art, widely-used air quality model is able to simulate the observations, as an indication for where there are still gaps in our knowledge and what further measurements and emissions dataset developments are needed. Model simulated regionally tagged CO tracers were used to identify emission source regions impacting pollutant concentration observed at Lumbini. Satellite data has also been used to understand the high pollution events during the monitoring period. These measurements were carried out as a part of the SusKat-ABC international air pollution measurement campaign (*M. Rupakheti, manuscript in preparation for ACPD*) jointly led by the International Centre for Integrated Mountain Development (ICIMOD), Kathmandu, Nepal and Institute for Advanced Sustainability Studies (IASS), Potsdam, Germany.

2. Experimental set up

2.1 Sampling site

The Lumbini measurement site (27º29.387′ N, 83º16.745′ E, elevation: ~100 m above sea level) is located at the premise of the Lumbini International Research Institute (LIRI), a Buddhist library in Lumbini of Rupandehi district. According to the National Census conducted in 2011, total population of Rupandehi district is about 900 thousand with the population density of about 650 person/square kilometer which is the fourth most densely populated district of the country. Over 130 thousand tourists visited Lumbini in 2014 (http://tourism.gov.np/en). A local road (black topped) lies about 200 m north of the sampling site and experiences intermittent passing of vehicles. About 25 km north of Lumbini the foothills begin while the main peaks of the

Himalayas are 140 km to the north. The remaining three sides are surrounded by flat plain land of Nepal and India. The site is only about 8 km from the Nepal-India border in the south. A three storied 10 m tall water tower was used as the platform for the automatic weather station (AWS) whereas remaining instruments were placed inside a room near the base of the tower. An uninterrupted power back up was set up in order to assure the regular power supply even during hours with scheduled power cuts during the monitoring period. Figure S1 shows the location of Lumbini, the Kenzo Tange Master Plan area of the Lumbini development project, the sampling tower and brief discussion on the surroundings of the site. Outside of the master plan area lie vast area of agricultural fields, village pockets, and several brick kilns and cement industries.

2.2 Monitoring Instruments

The summary of instruments deployed in Lumbini is presented in Table 1. All data were collected in Nepal Standard Time (NST) which is GMT +05:45 hour. PM_1, $PM_{2.5}$ and PM_{10} mass concentrations were monitored continuously with GRIMM EDM164 (GRIMM Aerosol Technik, Germany) which uses the light scattering at 655 nm to derive mass concentrations. Similarly, aerosol light absorptions at 7 wavelengths (370, 470, 520, 590, 660, 880, 950 nm) were measured continuously with an Aethalometer (Model AE-42, Magee Scientific, USA), averaging and reporting data every 5 min. It was operated at a flow rate of 5 l min^{-1}. No cut-off was applied for inlet; hence the reported concentration of BC is total suspended BC particles. As described by the manufacturer, ambient BC concentration is derived from light absorption at 880 nm using a specific mass absorption cross section. To obtain BC concentration in Lumbini, we used a specific mass absorption cross-section value of 8 m^2 g^{-1} for the 880 nm channel. A similar value has been previously used for BC measurement in the Indo-Gangetic plain (Praveen et al., 2012). To remove the filter loading effect, we used correction method suggested by Schmid et al. (2006) which was also used by Praveen et al. (2012) for BC measurements at a rural site in the Indo-Gangetic plain. Surface ozone (O_3) concentration was measured continuously with an ozone analyzer (Model 49*i*, Thermo Scientific, USA) which utilizes UV (254 nm wavelength) photometric technology to measure ozone concentration in ambient air. CO analyzer (Model 48*i*, Thermo Scientific, USA) was used to monitor ambient CO concentration. The ambient air was drawn through 6-micron pore size SAVILLEX 47 mm filter at the inlet in order to remove the particles before sending air into the CO and O_3 analyzers using a Teflon tube. The filters were

replaced every 7-10 days depending on particle loading, based on manual inspection. CO instrument was set to auto-zero at a regular interval of 6 hours. Local meteorological parameters (temperature, relative humidity, wind speed, wind direction, precipitation, and global solar radiation) were monitored with an automatic weather station (AWS) (Campbell Scientific, Loughborough, UK), recording data every minute.

2.3 Regional chemical transport model

Aerosol and trace gas distributions were simulated using a regional chemical transport model. Sulfur Transport and dEposition Model (STEM), a 3D eulerian model that has been used extensively in the past to characterize air pollutants in South Asian region (Adhikary et al., 2010; Adhikary et al., 2007) was used to understand observations at Lumbini. The Weather Research and Forecasting (WRF) model (Skamarock et al., 2008) version 3.5.1 was used to generate the required meteorological variables necessary for simulating pollutant transport in STEM. The model domain was centered at 24.94º N latitude and 82.55º E longitude covering a region from 3.390º N to 43.308º N latitude and 34.880º E to 130.223º E longitude. The model has 425×200 horizontal grid cells with grid resolution of 25 km × 25 km and 41 vertical layers with top of the model set at 50 mbar. The WRF model was run from November 1, 2012 to June 30, 2013. However, for this study, modeled data only from April to June 2013 have been used. The WRF model was initialized with FNL data available from NCAR/UCAR site (http://rda.ucar.edu/datasets/ds083.2/).

The tracer version of the STEM model provides mass concentration of sulfate, BC (hydrophilic and hydrophobic), Organic carbon (OC), sea salt (fine and coarse mode), dust (fine $PM_{2.5}$ and PM_{10}), CO (open burning and anthropogenic) and region tagged CO tracers. STEM model domain size, resolution and projection are those of the WRF model. Details about tracer version of the STEM model is outlined elsewhere (Kulkarni et al., 2015; Adhikary et al., 2007). Anthropogenic emission of various pollutants (CH_4, CO, SO_2, NO_x, NMVOC, NH_3, PM_{10}, $PM_{2.5}$, BC and OC) used in this analysis were taken from the EDGAR-HTAP_v2 (http://edgar.jrc.ec.europa.eu/htap_v2/index.php?SECURE=123) for 2010. Annual emissions given in kg/m^2/sec at 0.1x0.1 degree resolution were converted to molecules/cm^2/sec and re-gridded to 25 km x 25 km resolution using four point interpolation techniques available in the

197 STEM emission preprocessor. The emissions were given a diurnal profile using previously used
198 parameterization available in the preprocessor. Open biomass burning emissions on a daily basis
199 during the simulated period were taken from data obtained from the FINN model (Wiedinmyer et
200 al., 2011). As with the WRF model, the STEM model was run from November 2, 2012 to June
201 30, 2013 however, data presented here are only during the intensive field campaign period.

202 ## 3. Results and discussions

203 ### 3.1 Meteorology

204 Hourly average time series of various meteorological parameters like precipitation in mm hr^{-1}
205 (Prec), temperature in ºC (T), relative humidity in % (RH), wind speed in m s^{-1} (WS) and
206 direction in degree (WD) during the monitoring period are shown in Figure 2. Meteorological
207 parameters were obtained with the sensors at the height of ~12 m from the ground. Meteorology
208 results from WRF model simulations have been used to indicate if any significantly different air
209 mass type was present during the measurement campaign after the meteorological observations
210 malfunctioned. Precipitation data was derived from TRMM satellite (TRMM_3B42_007 at a
211 horizontal resolution of 0.25º) from the Giovanni platform
212 (http://giovanni.gsfc.nasa.gov/giovanni/) as the rain gauge malfuntioned during the sampling
213 period. Precipitation data from TRMM (Figure 2) show that Lumbini was relatively dry in the
214 early portion of the measurement campaign while as the pre-monsoon edged closer to the
215 monsoon onset, the site did experience some rainfall events. This lowered aerosol loading in the
216 later half of the measurement campaign due to washout and less biomass open burning.
217 Comparison of WRF model outputs with TRMM data shows that the model under-predicts
218 rainfall through out the campaign.

219 Average observed temperature for the sampling period until the sensor stopped working (on 8th
220 May, 2013, i.e., for 38 days of measurement) was 28.1ºC (minimum: 16.5ºC, maximum: 40ºC).
221 Average temperature from the model, during same period, was 31ºC with values ranging
222 between 19 - 40ºC. As shown in Figure 2, the model captures the variability of temperature and
223 is mostly within the range of daily values. However, the model has a high bias and does not
224 capture well daily minimum temperature values. The model data was interpolated to match the
225 observation site's latitude, longitude and altitude for all variables discussed in this paper. In

addition, the model does not show any large variation in temperature for the campaign period after the sensors stopped working. This insight will be useful to interpret pollution data later on. For the same period (until the sensor stopped working), the average (observed) RH was ~ 50% (ranging from 10.5 to 97.5%) whereas the model showed the average RH to be ~ 23% with values ranging between 6 to 78%. RH values are highly underestimated by the model, however as previously mentioned, the model does not show significant changes in RH during the measurement campaign after the observations stopped working.

Average observed wind speed during the study period was 2.4 m s^{-1}, with hourly values ranging between 0.03 - 7.4 m s^{-1} whereas from the WRF model average wind speed was found to be 3.2 m s^{-1} (range: 0.06 - 11.1 m s^{-1}). Diurnal variation of observed hourly average wind speed suggested that wind speeds were lower during nights and mornings while higher wind speed prevailed during day time, with average winds > 3 m s^{-1} up to ~ 3.3 m s^{-1} between 09:00-13:00 local time (Supplementary materials, Figure S2, lower panel). High speed strong winds (> 4 m s^{-1}) were from the NW direction during the month of April which later switched to almost opposite direction, i.e., SE direction from the month of May onwards. The monthly wind rose plot using the data from both observation and modeling where the difference in the pattern could be potentially due to the data resolution is shown in Figure S3. Comparing modeled wind direction prediction skills at the surface with one point measurement is not sufficient. However, in the absence of other measurements, we also show the comparison of wind direction as an indication of model performance over this region and not as model validation where a more high resolution modeling and sensitivity analysis of model physics and chemistry maybe required. Discrepancy on model results might have occurred due to various factors inherently uncertain in a weather prediction using a model. Besides, air pollution transport also occurs via elevated layers and is not limited to surface winds. We show NCEP/NCAR reanalysis plots at 850 hPa in Fig. S3 to illustrate the distinctly differing wind direction compared to the surface winds seen from observations as well as NCEP/NCAR reanalysis plot at 1000 hPa shown in Fig. 1. There are no upper wind measurement data nearby Lumbini to show model performance. Regardless, we believe that air quality model data is vital for understanding pollutant transport in an area where observation data are non-existent or are incomplete.

3.2 Air Quality

3.2.1 General overview, PM ratios and influence of meteorology on pollution concentrations

Figure 3 shows hourly averaged time series of observed BC, PM_1, $PM_{2.5}$, PM_{10}, O_3 and CO observed at Lumbini during the study period. Similar temporal behaviour was shown by BC, particulate matter fractions (PM_1, $PM_{2.5}$ and PM_{10}) and CO. The gap in the figure (for PM time series) is due to the power interruption to the instrument. BC concentrations during the measurement period ranged between 0.3-29.9 μg m^{-3} with a mean (±SD) value of 4.9 (±3.8) μg m^{-3}. BC concentrations in Lumbini during pre-monsoon months are lower compared to BC concentrations observed in the Kathmandu Valley because of high number of vehicles plying on the street, brick kilns and other industries in Kathmandu valley (Sharma et al., 2012; Putero et al., 2015). The lowest concentration was observed during a rainy day (21-22 April) whereas the highest concentration was observed during a period of forest fire (detailed in Section 3.3). For the entire measurement period, we found average (of hourly average values) PM_1: 35.8±25.6 μg m^{-3} (minimum-maximum range: 3.6 - 197.6 μg m^{-3}), $PM_{2.5}$: 53.1±35.1 μg m^{-3} (6.1 - 272.2 μg m^{-3}), PM_{10}: 128.9±91.9 μg m^{-3} (10.5-603.9 μg m^{-3}) and coarse-mode: 75.7±61.7 μg m^{-3} (1.9-331.8 μg m^{-3}). The coarse-mode ($PM_{10-2.5}$) fraction was ~ 60% of the PM_{10}. The share of coarse-mode aerosol to PM_{10} in Lumbini was higher than that observed in other sites in the IGP; Guwahiti, India (42%) (Tiwari et al., 2017) and Dibrugarh, India (9-16%) (Pathak et al., 2013) both in eastern IGP and Delhi (38%) (Tiwari et al., 2015) in western IGP indicating the higher contribution of coarse aerosols in Lumbini, likely lifted from soils from nearby agricultural fields and construction materials by stronger winds during pre-monsoon season. Similar value of coarse-mode fraction, as in Lumbini, has been reported by Misra et al. (2014) at Kanpur for dust dominated and mixed aerosols events.

The share of BC in PM fractions was found to be ~13% in PM_1, 9% in $PM_{2.5}$ and ~4% in PM_{10} but the correlation coefficients of BC with three PM fractions were found to be 0.89 (PM_1), 0.88 ($PM_{2.5}$) and 0.69 (PM_{10}), indicating the commonality in the sources of these pollutants. The contribution of BC in PM_1 was found to be of ~12% in Kanpur during February-March (Kumar et al., 2016a) similar to Lumbini. Regarding the share of BC in PM_{10}, the share observed in Lumbini (~4%) was similar to that observed over Varanasi (~340 km due south of our site) in central IGP (5%) (Tiwari et al., 2016) and Dibrugarh in eastern IGP (~5%) (Pathak et al., 2013).

Thus our results indicate that despite our station being located at the northern edge of the IGP along the foothills of the Himalayan range, the share of BC in PM are similar to those found in heavily polluted sites in the central and eastern IGP.

In Lumbini, the average (hourly) share of PM_1 in $PM_{2.5}$, PM_1 in PM_{10} and $PM_{2.5}$ in PM_{10} were found to be ~70%, 34% and 47% respectively. Regarding other sites in IGP region, $PM_{2.5}/PM_{10}$ ratios were reported to be 56% in Kanpur (Snider et al., 2016), 60% in Varanasi (Kumar et al., 2015), 57% in Guwahiti (Tiwari et al., 2017), 90% in Dribugarh (Pathak et al., 2013) and 62% in Delhi (Tiwari et al., 2015) indicating local differences within IGP as well as suggesting that influence of combustion sources at Lumbini is still lower compared to other locations in Indian section of the IGP. A recent study (Putero et al., 2015) reported the PM_1/PM_{10} during pre-monsoon of 2013 was found to be 0.39 in the Kathmandu Valley of Nepal. Lumbini has significantly lower vehicle emissions and population than the Kathmandu Valley yet the ratios are similar, indicating the importance of regional combustion sources in Lumbini for finer aerosols (PM_1), and soil-based emissions such as road dust in the Kathmandu Valley. Future studies will need to explore the emission sources around Lumbini in much greater detail. Lower $PM_{2.5}/PM_{10}$ in Lumbini as compared to other regions mentioned earlier could be due to emissions from cement industries located within 15 km distance from the measurement site.

The observed 24-hour average particulate matter concentrations ($PM_{2.5}$ and PM_{10}) were found frequently higher than the WHO prescribed guidelines for $PM_{2.5}$ (25 µg m^{-3}) and PM_{10} (50 µg m^{-3}) with PM2.5: exceeding 94% and PM_{10}: 85% of the measurement period of 53 days in Lumbini.

Observed CO concentrations ranged between 124.9-1429.7 ppbv with an average value of 344.1±160.3 ppbv. CO concentration observed in Lumbini is lower than that of Mohali, Western India where the average concentration was 566.7 ppbv during pre-monsoon season due to intense biomass and agro-residue burning over the region (Sinha et al., 2014). Temporal variation of CO concentrations is similar to that of BC exhibiting very strong correlation ($r = 0.9$). Past studies have shown that the ratio of BC to CO depends upon multiple factors like site location, combustion characteristics (fuel and technology) at the sources, and type of air mass (Girach et al., 2014; Pan et al., 2011; Zhou et al., 2009). Formation of the soot depends on the carbon to

oxygen ratio of fuel whereas CO can also be produced naturally due to the oxidation of VOCs (Girach et al., 2014). Figure 4 shows the comparison of the average ΔBC/ΔCO ratio (0.021) at Lumbini with that obtained from other sites. Please refer to Figure S4 in the supplementary materials for the time series of ΔBC/ΔCO ratio observed in Lumbini. We used the method described by Pan et al. (2011) to calculate the ΔBC/ΔCO values. The ratio was calculated using the equation $(BC-BC_0)/ (CO-CO_0)$ assuming the background values (BC_0 or CO_0) as 1.25 percentile of the data. The ΔBC/ΔCO ratio in Lumbini is similar to that obtained at a suburban site, Pantnagar in India (0.017) (Joshi et al., 2016) and in Maldives (0.017) (Dickerson et al., 2002) indicating the possibility of similar types of emission sources. However, lower ΔBC/ΔCO ratio obtained over megacities such as Beijing and Shanghai are due to the higher number of gasoline and diesel vehicles (Zhou et al., 2009). The ratios obtained at Lumbini are within the range of emission ratios from diesel used in transport sector (0.0013-0.055), coal (0.0019-0.0572) and biofuels (0.0087-0.0266) for domestic activities (Verma et al., 2010 and references therein) implying that BC and CO observed are from mixed sources.

The hourly averaged observed ozone concentration ranged between 1.0 and 118.1 ppbv with a mean value of 46.6±20.3 ppbv during the sampling period. The 8-hr maximum O_3 concentration exceeded WHO guidelines (of 100 µg m^{-3}; (WHO, 2006) during ~ 90% of the measurement period. Our results clearly indicate that the current pollution levels in Lumbini are of great concern to health of the people living in the region including over a million visitors who visit Lumbini, and agro-ecosystems.

The relationship of wind speed (WS) with aerosol and gaseous pollutants in Lumbini is shown in Figure S5 (Supplementary information). We were interested in studying the relationship between wind speed and the pollutants since the wind governs the horizontal dilution of the pollutants (Huang et al., 2012) and also likelihood of lifting soil dust. Except ozone, all other pollutants exhibited negative correlation with wind speed. BC shows negative correlation ($r = -0.42$, $P>0.05$) with the wind speed which is similar with other pollutants as well (as can be seen from the figure). Past studies have also reported a similar negative correlation of BC with wind speed over urban and sub-urban areas (Huang et al., 2012; Cao et al., 2009; Ramachandran and Rajesh, 2007; Sharma et al., 2002; Tiwari et al., 2013) indicating that the locally generated BC can accumulate in the atmosphere during lower wind speed conditions (Cao et al., 2009). Tiwari et

al. (2013) also reported similar negative correlation (r = -0.45) during the pre-monsoon season over Delhi. On the other hand, secondary pollutants like ozone exhibited a positive relation with the WS (r=0.38, P>0.05) indicating the location of precursor emission sources at some distance away from the measurement site. Solar radiation is one of the most important factors for production of ozone in the atmosphere (Naja et al., 2003). The correlation of hourly ozone concentration with solar radiation (not shown here) was found to be 0.41 (P>0.05) whereas wind speed during the daytime only (06:00-18:00) showed very weak correlation of 0.02 (non-significant) with ozone, possibly indicating transport of precursors during night time.

Interestingly, the highest concentrations of all measured pollutants were obtained when the wind speed was less than 1 m s^{-1}. In a separate analysis (not shown here), we considered only the WS >1 m s^{-1} and calculated the correlation coefficients to investigate the influence of regional emissions. We found the similar correlation values as previous when all WS values were considered (BC vs WS = -0.41, CO vs WS = -0.42, O_3 vs WS= 0.29, PM_1 vs WS= -0.40, $PM_{2.5}$ vs WS= -0.38, PM_{10} vs WS= -0.33 all at P>0.05). The correlation of WS (>1 m/s) with concentration of air pollutants elucidates that air pollution over Lumbini is not only of the local origin, it is rather transported from other nearby regions as well.

Past studies near this site have been focused on the cities like Kathmandu (Sharma et al., 2012; Ram et al., 2010; Panday and Prinn, 2009; Putero et al., 2015) and Kanpur (Ram et al., 2010) and agro-residue burning dominated regions of IGP (Rastogi et al., 2016; Sinha et al., 2014; Sarkar et al., 2013) all of which reported very high level of pollution. Our study adds to the growing list of scientific observations in the IGP by providing data in the foothills of central Himalayas. Very high aerosol loading is observed in South Asia during pre-monsoon, mostly over the IGP region (Supplementary materials, Figure S6). As this is the first study over an IGP site located in Nepal, pollution concentrations observed at Lumbini were compared with other sites in the region (Table 2). Different sites located at urban, semi-urban and remote locations were used for comparison to get a clear comparative picture of the situation at Lumbini amongst other locations in the region. Pre-monsoon seasonal average $PM_{2.5}$ concentration in Lumbini has been found to be lower than the megacity like Delhi (Bisht et al., 2015) and north-western IGP (Sinha et al., 2014), possibly due to higher level of emissions (from traffic and biomass burning, respectively) over those regions. In addition, average BC and CO concentrations in Lumbini were found falling in between concentrations observed at rural sites (up to 6 times higher) and cities in the

region (see Table 2), indicating that Lumbini, in a way, can still be considered as semi-urban location. The hourly average O_3 concentration in Lumbini were found to be higher than the cities like Kathmandu (Putero et al., 2015) and Kanpur during pre-monsoon season (Gaur et al., 2014). However from a mesoscale perspective, the hourly average O_3 concentrations were lower at Lumbini as compared to base camp of Mt. Everest region due to the uplift of polluted air masses (Marinoni et al., 2013), stratospheric intrusion (Cristofanelli et al., 2010) and even the regional or long-range transport of the air pollutants (Bonasoni et al., 2010) to the high altitude site.

Regarding the monthly average concentration, the concentrations of all measured pollutants decreased as the pre-monsoon months advanced. The monthly average concentrations of the monitored species are shown in Figure S7 along with the monthly fire hotspots over the region. Reduction in concentration (except PM) during the month of May (as compared to April) could be attributed to the fewer fire events during May as well as previously discussed washout by rainfall. Two peak pollution episodes observed during the first half of April and May which are discussed in more detail in the next section.

3.2.2 Observation-model inter-comparison

Chemical transport models provide insight to observed phenomena; however, interpretation has to take into account model performance before arriving at any conclusion. This section describes pollution concentrations simulated by the WRF-STEM model. A comparison of model calculated pollutant concentration along with the minimum and maximum concentrations of various pollutants (with observation) is shown in Table 3. The model based concentrations used here are values outputted for every third hour of the day (actual computation is carried out every 15 minutes). BC concentrations ranged between 0.4-3.7 μg m^{-3} with a mean value of 1.8±0.7 μg m^{-3} for a period of 1st April-15th June 2013. The average model BC concentration was ~2.7 times lower than the observed BC. Regarding PM_1, $PM_{2.5}$ and PM_{10}, the model simulated average concentration was 12.3±5.5 (0.9-41.7) μg m^{-3}, 17.3±6.7 (1.9-48.3) μg m^{-3} and 25.4±12.9 (2.1-68.8) μg m^{-3}, respectively. The model estimated values were lower by the factor of 3 and 5 respectively than the observed concentrations. The data show that model needs much improvement in its ability to adequately predict observed aerosol characteristics at Lumbini given the input provided, for example, emissions data. Since pollutant concentration is a function

of emissions, transport and transformation and deposition, improvements in any of these areas would improve the model performance for this site. However, given observation insights by PM ratios, it seems that improvements are much needed in the emissions of primary aerosols. Current emissions (2010) do not account for trash burning, roadside dust and increasingly newer industries, especially emissions from cement factories that have propped up in recent years. We show sensitivity with emissions in a later section (3.3.2) in the vicinity of Lumbini, however emission improvements are needed beyond Lumbini which is outside the scope of this paper.

Average observed CO concentration was 255.7±83.5 ppbv, ranging between 72.2-613.1 ppbv, with average model CO ~1.35 times lower than observed. Time series comparison of modeled CO versus observation is shown in Figure 3. Apart from two peak episodes the model does a better job in predicting CO concentration over Lumbini. Previous study using the STEM model over Kathmandu valley showed that the model was able to capture annual BC mean value but completely missed the concentrations during pre-monsoon and post monsoon period (Adhikary et al., 2007). Similar behavior is seen this time for CO where the model misses the peak values but reasonably captures CO concentration after mid-May when no biomass burning events are observed (model to observation ratio improves to 1.16). STEM model CO performance can be significantly improved via better constraining emissions of open biomass burning as discussed in Section 3.3. This activity is beyond the scope of this current paper although the improvements are underway for all these sectors.

3.2.3 Diurnal variations of air pollutants and boundary layer height

In the emission source region, diurnal variations of primary pollutants provide information about the time dependent emission activities (Kumar et al., 2016b). Figure 5 shows the diurnal variation of hourly averaged concentrations of measured pollutants during the sampling period. Primary pollutants like BC, PM and CO showed typical characteristics of an urban environment, i.e., diurnal variation with a morning and an evening peak. However, Lumbini data shows higher concentrations in the evenings compared to morning hours. Elevated concentrations can be linked to morning and evening cooking hours for BC and CO. Emission inventory for the region show that residential sector has significant contribution to BC and CO. However, explanation for elevated evening concentration compared to morning needs further investigation. Increase in the

boundary layer height, reduction in the traffic density on the roads, absence of cooking activities during mid-day and increasing wind speed often contribute to the dispersion of pollutants resulting in lower concentration during afternoon. Diurnal variation of wind direction (Supplementary information, Figure S2, upper panel) shows the dominance of wind coming from south (mainly during the month of May and till mid-June). Morning and evening period experienced the winds coming from the southeast direction while the winds were predominantly from southwest direction during late afternoon. Increase in CO concentrations in the evening hours might be due to transport of CO from source regions upwind of Lumbini which along with the local emissions gets trapped under reduced Planetary Boundary Layer (PBL) heights. Ozone concentration was lowest in the morning before the sunrise and highest in late afternoon around 15:00 PM after which concentrations started declining, exhibiting a typical characteristic of a polluted urban site. Photo-dissociation of accumulated NO_x reservoirs (like HONO) provides sufficient NO concentration leading to the titration of O_3 resulting in minimum O_3 just before sunrise (Kumar et al., 2016b). The PBL height (in meters (m)) was obtained from the WRF model as observations were not available. The study period average PBL height over Lumbini was ~ 910 m (ranging between 24 and 3807 m observed at 06:00 and 15:00 respectively). The daily average PBL height obtained from the model is compared with published values (Wan et al., 2017) as shown in Figure 6, which indicate that the value is captured by our model during initial measurement period and overestimated in the months of mid May onwards. As the pre-monsoon month advances, PBL height also increased. The monthly average PBL height was 799 m, 956 m and 1014 m respectively during the month of April, May and (1^{st}-15^{th}) June. As presented in the figure, the monthly average diurnal variation also showed that the boundary layer height was maximum during 15:00 local time during each month which coincides with the period of lowest concentration of the pollutants.

3.3 Influence of forest fires on Lumbini air quality

3.3.1 Identification of forest fire influence over large scale using in-situ observations, satellite and model data

Forest fires and agricultural biomass burning (mostly agro-residue burning in large scale) are common over the South Asia and the IGP region during pre-monsoon season. North Indo-

Gangetic region is characterized by fires even during the monsoon and post-monsoon season (Kumar et al., 2016b; Putero et al., 2014). These activities influence air quality not only over nearby regions but also get transported towards high elevation pristine environments like Mt. Everest (Putero et al., 2014) and Tibet (Cong et al., 2015a; 2015b). So, one of the main objectives of this study was to identify the influence of open burning on Lumbini air quality. Average wind speed during the whole measurement period was 2.4 m s^{-1}. Based on this data, open fire counts within the grid size of 200×200 km centering over Lumbini was used for this analysis assuming that the emissions will take a maximum period of one day to reach our monitoring site. Forest fire counts were obtained from MODIS satellite data product Fire Information for Resource Management System (FIRMS). Figure 7 shows the daily average ΔBC/ΔCO ratio, aerosol absorption Ångstrom exponent (AAE) which is derived from Aethalometer data (by calculating the negative slope of absorption at 370 nm and 950 nm versus wavelength in log-log plot) and daily open fire count within the specified grid. The green box in the figure is used to show two peak events (presented earlier in Fig. 3) with the elevated BC and CO concentrations observed during the monitoring period. The first peak was observed during 7-9 April and second peak during 3-4 May, 2013. Two pollutants having biomass burning as the potential primary source: BC and CO were taken in consideration. High AAE values during these two events are also an indication of presence of BC of biomass burning origin (Praveen et al., 2012; Bergstrom et al., 2007; Kirchstetter et al., 2004), with the value being ~ 1.6 for Lumbini. The chemical composition of TSP filter samples collected at Lumbini also showed higher concentration of Levoglucosan, a biomass burning tracer in Lumbini during the pre-monsoon season as compared to other seasons of the year (Wan et al., 2017). Wan et al. (2017) also reported that the higher correlation between K^+ with Ca^{2+} and Mg^{2+} indicating that dust is the main source of potassium in Lumbini.

Contrary to our expectation, we could not observe any significant influence of forest fire within the specified grid of 200x200 km (or the influence of local forest fire on the air quality over Lumbini was not observed). Therefore, a wider area, covering South and Southeast Asian regions, was selected for the forest fire count. Figure 8 (A-B) shows the active fire hotspots from MODIS, over the region, during the peak events which shows the first peak could have occurred due to the forest fire over the eastern India region whereas the second peak was influenced by the

493 forest fire over western IGP region. Moreover, in order to strengthen our hypothesis, we have
494 utilized satellite data products for various gaseous pollutants like CO and NO_2 (Atmospheric
495 Infrared Sounder (AIRS) for CO and Ozone Monitoring Instrument (OMI) for NO_2 both
496 obtained from Giovanni platform). Figure 8 (C-H) shows the daytime total column CO before,
497 during and after occurrence of two events (peaks) as stated earlier. Atmospheric Infrared
498 Sounder (AIRS) satellite with daily temporal resolution and $1^o \times 1^o$ spatial resolution have been
499 utilized to understand the CO concentration over the area. CO concentration over Lumbini
500 during both of the peaks confirmed the role of open fires over the IGP region for elevated
501 concentration of CO in Lumbini. To further strengthen our finding, the aid of HYSPLIT back
502 trajectories plots was taken. Figure 8 (I-J) represent the 6-hourly back trajectories only for these
503 two events respectively. However, the back trajectories (during both events) indicated that the air
504 mass passed over the fire events in the north western IGP. We note that using back trajectories to
505 identify source regions are also uncertain as identified by Jaffe et al. (1997). Figure 8 (K) shows
506 model biomass CO peak coincident with observed CO. Although the magnitudes are
507 significantly different, the timing of the peaks is well captured by the model. This, we believe, is
508 due to the fact that satellite based open fire detection also has limitation as it does not capture
509 numerous small fires that are prevalent over south Asia which usually burn out before the next
510 satellite overpass. More research is needed to assess the influence of these small fires on regional
511 air quality.

512 In a separate analysis (not shown here), elevated O_3 concentration during these two events were
513 also observed. Average O_3 concentration before, during and after the events were found to be
514 46.2±20.3 ppbv, 53.5±31.1 ppbv and 50.3±20.9 ppbv respectively (Event-I) whereas it was
515 found to be 54.8±23.8 ppbv, 56.7±35 ppbv and 55.6±13.4 ppbv respectively (Event-II). Average
516 ozone concentration outside these events was found to be 46±19 ppbv. Increased ozone
517 concentrations during the high peak events have been analyzed using the satellite NO_2
518 concentration over the region considering the role of NO_2 as precursor for ozone formation.
519 Daily total column NO_2 were obtained from OMI satellite (data available at the Giovanni
520 platform; http://giovanni.gsfc.nasa.gov/giovanni/) at the spatial resolution of $0.25^o \times 0.25^o$. Figure
521 9 shows the NO_2 column value before, during and after both events. Even for the NO_2, maximum
522 concentrations were observed during these two special events. It is likely that the local as well as

regional pollution (transported from NW IGP region as indicated by synoptic wind in Figure S8) contributed to the elevated ozone levels. This remains a question to be investigated in future.

3.3.2 Identifying regional and local contribution

WRF-STEM model has been used to identify the anthropogenic emission source region influencing the air quality over Lumbini. As previously explained, the model is able to capture the observed CO concentration when intense open burning events were not present. A recent study (Kulkarni et al., 2015) has explored the source region contribution of various pollutants over the Central Asia using similar technique. Figure 10 (A) shows the average contribution from different regions on CO concentration over Lumbini during the whole measurement period. Major share of CO was from the Ganges valley (46%) followed by Nepal region (25%) and rest of Indian region (~17.5%). Contribution from other South Asian countries like Bangladesh and Pakistan were ~ 11% whereas China contributed for ~1% of the CO concentration in Lumbini. Regarding the monthly average contribution, the Ganges Valley and Nepal's contribution were almost equal during the month of April (~34% and ~37% respectively) but increased for the Ganges Valley region during the month of May (~44%) and got reduced for Nepal region (~25%) (Figure S9).

Figure 10 (B) is the time series of percentage contribution to total CO concentration during whole measurement period showing different air mass arriving at a 3 hourly intervals. During the whole measurement period, majority of the CO reaching Lumbini were from the Ganges valley (mainly the states of Punjab, Haryana, Uttar Pradesh, Bihar and West Bengal) region with the contribution sometimes reaching up to ~80%. Other India (central, south, east and north) regions also contributed significantly. Bangladesh's contribution in CO loading was seen only after mid-April lasting for only about a week and after the first week of May. The contribution from Bangladesh was sporadic comparing to other regions. Highest contribution from this Bangladesh region was observed after the first week of June with the arrival of monsoonal air mass. Pakistan also contributed for the CO loading significantly. Others region as mentioned in the figure covered the regions like Afghanistan, Middle east, West Asia, East Asia, Africa and Bhutan. Contributions from these regions were less than 5%. Contribution from China was not evident

till the first week of June where a specific air mass arrival shows contribution reaching up to 25% of total CO loading.

A sensitivity analysis was performed for emission uncertainty in the model grid containing Lumbini. Lumbini and surrounding regions in the recent years has seen significant rise in urban activities and industrial activity and related emissions which may not be accurately reflected in the HTAPv2 emissions inventory. A month long simulation was carried out with emissions from Lumbini and the surrounding four grids off and another simulation with Lumbini and surrounding four grid's emissions increased by 5 times the amount from HTAPv2 emissions inventory. The results are shown in Figure 10 (C) as percentage increase or decrease compared to model results using the current HTAPv2 emissions inventory. The black line shows concentration as 100% for the current HTAPv2 emissions inventory. Despite making Lumbini and the surrounding grids emissions zero, model calculation shows pollutant concentration on average is still about 78% of the original value indicating dominance of background and regional sources compared to local source in the model. Increasing emissions 5 times for the Lumbini and surrounding four grids only increases the concentration on average by 151%. Thus uncertainty in emissions are not a local uncertainty for Lumbini rather for the whole region which needs to be better understood for improving model performance against observations at Lumbini.

3.4 Does fossil fuel or biomass influence the Lumbini air?

The aerosol spectral absorption is used to gain insight into nature and potential source of black carbon. This method enables to analyze the contributions of fossil fuel combustion and biomass burning contributions to the observed BC concentration (Kirchstetter et al., 2004). Besides BC, other light absorbing (in the UV region) aerosols are also produced in course of combustion, collectively termed as organic aerosols (often also called brown carbon or BrC) (Andreae and Gelencsér, 2006). Figure 11 shows the comparison of normalized light absorption as function of the wavelength for BC observed at Lumbini during cooking and non-cooking hours and also for the both events. Our results are compared with the published data of Kirchstetter et al. (2004) and that observed over a village center site of Project Surya in the IGP (Praveen et al., 2012) (figure not shown). We discuss light absorption data from two distinct times of the day. The main reason behind using data during 07:00-08:00 h and 16:00-17:00 h is these periods represent

highest and lowest ambient concentration (Fig. 5). Also these period represent cooking (07:00-08:00 h) and non-cooking (16:00-17:00 h) or high and low vehicular movement hours (Praveen et al., 2012). To understand the influence of biomass and fossil fuel we plotted normalized aerosol absorption at 700 nm wavelength for complete aethalometer measured wavelengths in Fig. 11. Kirchstetter et al. (2004) reported OC absorption efficiency at 700 nm to be zero. Thus we normalized measured absorption spectrum by 700 nm wavelength absorption. Since aethalometer does not provide 700 nm wavelength absorption values, we calculated the value using the absorption at nearby wavelengths and angstrom exponent following the methodology used by Praveen et al. (2012). Our results show that the normalized absorption for biomass burning aerosol is ~3 times higher at 370 nm compared to that at 700 nm whereas fossil fuel absorption is about 2.6 times higher at the same wavelength. In addition, the curve obtained for the both events are inclined towards the published biomass burning curve. The normalized curve obtained during both cooking and non-cooking period lies in between the standard curve of Kirchstetter et al. (2004). As shown in Fig. 11, the curve obtained for the prime cooking time is closer towards the published curve on biomass burning whereas that obtained during the non-cooking time is closer towards the published fossil fuel curve. Similar result was also observed over the Project Surya village in the IGP region (Praveen et al., 2012; Rehman et al., 2011). This clearly indicates there is contribution of both sources: biomass as well as fossil fuel on the observed BC concentration over Lumbini.

In order to identify fractional contribution of biomass burning and fossil fuel combustion to observed BC aerosol, we adopted the method described by Sandradewi et al. (2008). Wavelength dependence of aerosol absorption coefficient (b_{abs}) is proportional to $\lambda^{-\alpha}$ where λ is the wavelength and α is the absorption Ångstrom exponent. The α values ranges from 0.9-2.2 for fresh wood smoke aerosol (Day et al., 2006) and between 0.8-1.1 for traffic or diesel soot (references in Sandradewi et al. (2008)). We have taken α value of 1.86 for biomass burning and 1.1 for fossil fuel burning as suggested by previous literature (Sandradewi et al., 2008). Figure 12 shows diurnal variation of the biomass burning BC. Minimum contribution of biomass burning to total BC concentration was observed during 04:00-06:00 local time (only about 30% of the total BC). As the cooking activities start in morning, the contribution of biomass BC starts to increase and reaches about 50%. Similar pattern was repeated during evening cooking hours.

Only during these two cooking periods, fossil fuel fraction BC was lower. Otherwise it remained significantly higher than biomass burning BC throughout the day. On average, ~40% of BC was from biomass burning whereas remaining 60% was contributed by fossil fuel combustion during our measurement period. Interestingly, this is the opposite of the contributions that were concluded by Lawrence and Lelieveld (2010). Lawrence and Lelieveld (2010) concluded that ~60% BC from biomass versus ~40% fossil fuel, based on a review of numerous previous studies to be likely for the outflow from Southern Asia during the winter monsoon. When we compared observed Ångstrom exponent with Praveen et al. (2012), we noticed that Lumbini values were lower than Project Surya Village center site. This implies Surya village center had higher biomass fraction, also it was observed absorption Ångstrom exponent exceeded 1.86 during cooking hours which indicates 100% biomass contribution. The difference is attributed to the fact that Lumbini sampling site is not a residential site like Surya village which can capture cooking influence efficiently. Further Lumbini sampling site is surrounded by commercial activities such as a local bus park, hotels, office buildings and industries and brick kilns slightly further away. Although the reason for this difference is not clear, it is an indication of the important role of diesel and coal emissions in the Lumbini and upwind regions.

4. **Conclusions**

Our measurements, a first for the Lumbini area, have shown very high air pollution at Lumbini. Black carbon (BC), carbon monoxide (CO), ozone (O_3) and particulate matter (PM_{10}, $PM_{2.5}$ and PM1) were measured during the pre-monsoon of 2013 as a regional site of the *SusKat-ABC campaign*. Average pollutant concentrations during the monitoring period were found to be: BC: 4.9±3.8 μg m^{-3}; CO: 344.1±160.3 ppbv; O_3: 46.6±20.3 ppbv; PM_{10}: 128.8±91.9 μg m^{-3}, $PM_{2.5}$: 53.14±35.1 μg m^{-3} and PM_1: 36.6±25.7 μg m^{-3} which is comparable with other urban sites like Kanpur and Delhi in the IGP region. However, our study finds higher fraction of coarse mode PM in Lumbini as compared to other sites in the IGP region. In addition, ΔBC/ΔCO ratio obtained in Lumbini was within the range of emission from both residential and transportation sectors, indicating them as potential key sources of BC and CO, and likely most of PM_1 in Lumbini. The diurnal variation of the pollutants is similar to that of any urban location, with peaks during morning and evening. However, our results show higher evening concentration compared to morning concentration values and needs further research to explain this behavior.

During our measurement period, air quality in Lumbini was influenced by regional forest fires as shown by chemical transport model and satellite data analysis. A regional chemical transport model, WRF-STEM was used to understand observations. Inter-comparison of WRF-STEM model outputs with observations showed that the model underestimated the observed pollutant concentrations by a factor of ~ 1.5 to 5 but was able to capture the temporal variability. Model uncertainties are attributed mostly to uncertainties in meteorology and regional emissions as shown from sensitivity analysis with local emissions. Region-tagged CO as air-mass tracers are employed in WRF-STEM model to understand the anthropogenic emission source region influencing Lumbini. Our analysis shows that the adjacent regions; mostly the Ganges valley, other parts of India and Nepal accounted for the highest contribution to pollutant concentration in the Lumbini. The normalized light absorption curve clearly indicated the contribution to BC in Lumbini from both sources: biomass as well as fossil fuel. On average, ~40% BC was found to be from the biomass burning and ~60% from fossil fuel burning.

Various improvements and extensions would be possible in future studies. More reliable functioning of the AWS (temperature and RH sensor, rain gauge) would have allowed more in-depth analysis of the relationship between meteorological parameters and pollutants concentration. Continuous measurements of air pollutants throughout the year would allow for annual and seasonal variation study. Improvements in the model performance are much needed in its ability to simulate observed meteorology. Significant uncertainty lies with regional emissions inventory developed at national and continental scale versus local bottoms up inventory and pollutant emissions from small scale open burning not captured by satellites. There is a clear need for setting up of a continuous air quality monitoring station at Lumbini and the surrounding regions for long-term air quality monitoring.

Data availability

The observation data used for this manuscript can be obtained by sending an email to the corresponding authors and/or to IASS (Maheswar.Rupakheti@iass.potsdam.de) and/or to ICIMOD (arnico.panday@icimod.org). Modeling data can be obtained from B. Adhikary (Bhupesh.adhikary@icimod.org).

Authors' contributions

669 M.R. and M.L. conceived the Lumbini portion of the SusKat experiment. M.R. and A.K.P.
670 coordinated the Lumbini field campaign. D.R. and K.S.M conducted the field observations at
671 Lumbini. B.A. designed and ran the WRF-STEM model. P.S.P., B.A. and D.R. finalized the
672 manuscript composition. D.R., P.S.P, B.A., M.R. and S.K. conducted the data analysis. D.R. and
673 B.A. prepared the manuscript with inputs from all coauthors.

674 **Acknowledgements**

675 This study was partly supported by the Institute for Advanced Sustainability Studies (IASS),
676 Germany, the International Centre for Integrated Mountain Development (ICIMOD), and the
677 National Natural Science Foundation of China (41121001, 41225002), and the Strategic Priority
678 Research Program (B) of the Chinese Academy of Sciences (XDB03030504). Dipesh Rupakheti
679 is supported by CAS-TWAS President's Fellowship for International PhD Students. The IASS is
680 grateful for its funding from the German Federal Ministry for Education and Research (BMBF)
681 and the Brandenburg Ministry for Science, Research and Culture (MWFK). ICIMOD authors
682 would like to acknowledge that this study was partially supported by core funds of ICIMOD
683 contributed by the governments of Afghanistan, Australia, Austria, Bangladesh, Bhutan, China,
684 India, Myanmar, Nepal, Norway, Pakistan, Switzerland, and the United Kingdom. The views and
685 interpretations in this publication are those of the authors and are not necessarily attributable to
686 the institutions they are associated with. We thank B. Kathayat, B.R. Bhatta, and Venerable
687 Vivekananda and his colleagues (Panditarama Lumbini International Vipassana Meditation
688 Center) for providing logistical support which was vital in setting up and running the site. We
689 also thank C. Cüppers and M. Pahlke of the Lumbini International Research Institute (LIRI) for
690 proving the space and power to run the instruments at the LIRI premises. Satellite data providers
691 (MODIS, AIRS, OMI) and HYSPLIT team are also equally acknowledged.

692

References

Adhikary, B., Carmichael, G. R., Tang, Y., Leung, L. R., Qian, Y., Schauer, J. J., Stone, E. A., Ramanathan, V., and Ramana, M. V.: Characterization of the seasonal cycle of south Asian aerosols: A regional-scale modeling analysis, Journal of Geophysical Research, 112, D22S22, 1-22, 10.1029/2006jd008143, 2007.

Adhikary, B., Carmichael, G. R., Kulkarni, S., Wei, C., Tang, Y., D'Allura, A., Mena-Carrasco, M., Streets, D. G., Zhang, Q., Pierce, R. B., Al-Saadi, J. A., Emmons, L. K., Pfister, G. G., Avery, M. A., Barrick, J. D., Blake, D. R., Brune, W. H., Cohen, R. C., Dibb, J. E., Fried, A., Heikes, B. G., Huey, L. G., O'Sullivan, D. W., Sachse, G. W., Shetter, R. E., Singh, H. B., Campos, T. L., Cantrell, C. A., Flocke, F. M., Dunlea, E. J., Jimenez, J. L., Weinheimer, A. J., Crounse, J. D., Wennberg, P. O., Schauer, J. J., Stone, E. A., Jaffe, D. A., and Reidmiller, D. R.: A regional scale modeling analysis of aerosol and trace gas distributions over the eastern Pacific during the INTEX-B field campaign, Atmos. Chem. Phys., 10, 2091-2115, 10.5194/acp-10-2091-2010, 2010.

Andreae, M. O., and Gelencsér, A.: Black carbon or brown carbon? The nature of light-absorbing carbonaceous aerosols, Atmos. Chem. Phys., 6, 3131-3148, doi: 10.5194/acp-6-3131-2006, 2006.

Bergin, M. H., Tripathi, S. N., Jai Devi, J., Gupta, T., McKenzie, M., Rana, K., Shafer, M. M., Villalobos, A. M., and Schauer, J. J.: The Discoloration of the Taj Mahal due to Particulate Carbon and Dust Deposition, Environ. Sci. Technol., 49, 808-812, doi: 10.1021/es504005q, 2015.

Bergstrom, R. W., Pilewskie, P., Russell, P., Redemann, J., Bond, T., Quinn, P., and Sierau, B.: Spectral absorption properties of atmospheric aerosols, Atmospheric Chemistry and Physics, 7, 5937-5943, 2007.

Bisht, D. S., Dumka, U. C., Kaskaoutis, D. G., Pipal, A. S., Srivastava, A. K., Soni, V. K., Attri, S. D., Sateesh, M., and Tiwari, S.: Carbonaceous aerosols and pollutants over Delhi urban environment: Temporal evolution, source apportionment and radiative forcing, Sci. Total Environ., 521-522C, 431-445, doi: 10.1016/j.scitotenv.2015.03.083, 2015.

Bonasoni, P., Laj, P., Marinoni, A., Sprenger, M., Angelini, F., Arduini, J., Bonafè, U., Calzolari, F., Colombo, T., Decesari, S., Di Biagio, C., di Sarra, A. G., Evangelisti, F., Duchi, R., Facchini, M. C., Fuzzi, S., Gobbi, G. P., Maione, M., Panday, A., Roccato, F., Sellegri, K., Venzac, H., Verza, G. P., Villani, P., Vuillermoz, E., and Cristofanelli, P.: Atmospheric Brown Clouds in the Himalayas: first two years of continuous observations at the Nepal Climate Observatory-Pyramid (5079 m), Atmospheric Chemistry and Physics, 10, 7515-7531, doi: 10.5194/acp-10-7515-2010, 2010.

Brimblecombe, P.: The effects of air pollution on the built environment, Imperial College Press, London, 2003.

730 Burney, J., and Ramanathan, V.: Recent climate and air pollution impacts on Indian agriculture,
731 Proc. Natl. Acad. Sci. USA, 111, 16319-16324, doi: 10.1073/pnas.1317275111, 2014.

732 Cao, J.-J., Zhu, C.-S., Chow, J. C., Watson, J. G., Han, Y.-M., Wang, G.-h., Shen, Z.-x., and An,
733 Z.-S.: Black carbon relationships with emissions and meteorology in Xi'an, China,
734 Atmospheric Research, 94, 194-202, http://dx.doi.org/10.1016/j.atmosres.2009.05.009,
735 2009.

736 Cong, Z., Kang, S., Kawamura, K., Liu, B., Wan, X., Wang, Z., Gao, S., and Fu, P.:
737 Carbonaceous aerosols on the south edge of the Tibetan Plateau: concentrations,
738 seasonality and sources, Atmospheric Chemistry and Physics, 15, 1573-1584, doi:
739 10.5194/acp-15-1573-2015, 2015a.

740 Cong, Z., Kawamura, K., Kang, S., and Fu, P.: Penetration of biomass-burning emissions from
741 South Asia through the Himalayas: new insights from atmospheric organic acids,
742 Scientific Reports, 5, 1-7, doi: 10.1038/srep09580, 2015b.

743 Cristofanelli, P., Bracci, A., Sprenger, M., Marinoni, A., Bonafè, U., Calzolari, F., Duchi, R.,
744 Laj, P., Pichon, J. M., Roccato, F., Venzac, H., Vuillermoz, E., and Bonasoni, P.:
745 Tropospheric ozone variations at the Nepal Climate Observatory-Pyramid (Himalayas,
746 5079 m a.s.l.) and influence of deep stratospheric intrusion events, Atmospheric
747 Chemistry and Physics, 10, 6537-6549, doi: 10.5194/acp-10-6537-2010, 2010.

748 Das, S. K., and Jayaraman, A.: Role of black carbon in aerosol properties and radiative forcing
749 over western India during premonsoon period, Atmos. Res., 102, 320-334, doi:
750 10.1016/j.atmosres.2011.08.003, 2011.

751 Day, D., Hand, J., Carrico, C., Engling, G., and Malm, W.: Humidification factors from
752 laboratory studies of fresh smoke from biomass fuels, J. Geophys. Res., 111, D22202,
753 doi: 10.1029/2006JD007221, 2006.

754 Dickerson, R. R., Andreae, M. O., Campos, T., Mayol-Bracero, O. L., Neusuess, C., and Streets,
755 D. G.: Analysis of black carbon and carbon monoxide observed over the Indian Ocean:
756 Implications for emissions and photochemistry, Journal of Geophysical Research:
757 Atmospheres, 107, INX2 16-11-INX12 16-11, 10.1029/2001JD000501, 2002.

758 Duchi, R., Cristofanelli, P., Marinoni, A., Laj, P., Marcq, S., Villani, P., Sellegri, K., Angelini,
759 F., Calzolari, F., Gobbi, G. P., Verza, G. P., Vuillermoz, E., Sapkota, A., and Bonasoni,
760 P.: Continuous observations of synoptic-scale dust transport at the Nepal Climate
761 Observatory-Pyramid (5079 m a.s.l.) in the Himalayas, Atmos. Chem. Phys. Discuss., 11,
762 4229-4261, doi: 10.5194/acpd-11-4229-2011, 2011.

763 Forouzanfar, M. H., Alexander, L., Anderson, H. R., Bachman, V. F., Biryukov, S., Brauer, M.,
764 Burnett, R., Casey, D., Coates, M. M., and Cohen, A.: Global, regional, and national
765 comparative risk assessment of 79 behavioural, environmental and occupational, and
766 metabolic risks or clusters of risks in 188 countries, 1990–2013: a systematic analysis for

767 the Global Burden of Disease Study 2013, Lancet, 386, 2287-2323, doi: 10.1016/S0140-
768 6736(15)00128-2, 2015.

769 Ganguly, D., Jayaraman, A., Rajesh, T. A., and Gadhavi, H.: Wintertime aerosol properties
770 during foggy and nonfoggy days over urban center Delhi and their implications for
771 shortwave radiative forcing, Journal of Geophysical Research, 111, 1-15,
772 10.1029/2005jd007029, 2006.

773 Gaur, A., Tripathi, S. N., Kanawade, V. P., Tare, V., and Shukla, S. P.: Four-year measurements
774 of trace gases (SO_2, NO_x, CO, and O_3) at an urban location, Kanpur, in Northern India,
775 Journal of Atmospheric Chemistry, 71, 283-301, doi: 10.1007/s10874-014-9295-8, 2014.

776 Gauri, K. L., and Holdren, G.: Pollutant effects on stone monuments, Environ. Sci. Technol., 15,
777 386-390, doi: 10.1021/es00086a001, 1981.

778 Girach, I. A., Nair, V. S., Babu, S. S., and Nair, P. R.: Black carbon and carbon monoxide over
779 Bay of Bengal during W_ICARB: Source characteristics, Atmospheric Environment, 94,
780 508-517, http://dx.doi.org/10.1016/j.atmosenv.2014.05.054, 2014.

781 Huang, X.-F., Sun, T.-L., Zeng, L.-W., Yu, G.-H., and Luan, S.-J.: Black carbon aerosol
782 characterization in a coastal city in South China using a single particle soot photometer,
783 Atmospheric Environment, 51, 21-28, 10.1016/j.atmosenv.2012.01.056, 2012.

784 IPCC: Climate Change 2013: The Physical Science Basis. Contribution of Working Group I to
785 the Fifth Assessment Report of the Intergovernmental Panel on Climate Change [Stocker,
786 T.F., D. Qin, G.-K. Plattner, M. Tignor, S.K. Allen, J. Boschung, A. Nauels, Y. Xia, V.
787 Bex and P.M. Midgley (eds.)]. Cambridge University Press, Cambridge, United Kingdom
788 and New York, NY, USA, 1535 pp., 2013.

789 Jaffe, D., Mahura, A., Kelley, J., Atkins, J., Novelli, P. C., and Merrill, J.: Impact of Asian
790 emissions on the remote North Pacific atmosphere: Interpretation of CO data from
791 Shemya, Guam, Midway and Mauna Loa, Journal of Geophysical Research, 102, 28627,
792 10.1029/96jd02750, 1997.

793 Joshi, H., Naja, M., Singh, K., Kumar, R., Bhardwaj, P., Babu, S. S., Satheesh, S., Moorthy, K.
794 K., and Chandola, H.: Investigations of aerosol black carbon from a semi-urban site in the
795 Indo-Gangetic Plain region, Atmos. Environ., 125, 346-359, doi:
796 10.1016/j.atmosenv.2015.04.007, 2016.

797 Kirchstetter, T. W., Novakov, T., and Hobbs, P. V.: Evidence that the spectral dependence of
798 light absorption by aerosols is affected by organic carbon, Journal of Geophysical
799 Research, 109, 1-12, doi:10.1029/2004JD004999, 2004.

800 Kulkarni, S., Sobhani, N., Miller-Schulze, J. P., Shafer, M. M., Schauer, J. J., Solomon, P. A.,
801 Saide, P. E., Spak, S. N., Cheng, Y. F., Denier van der Gon, H. A. C., Lu, Z., Streets, D.
802 G., Janssens-Maenhout, G., Wiedinmyer, C., Lantz, J., Artamonova, M., Chen, B.,
803 Imashev, S., Sverdlik, L., Deminter, J. T., Adhikary, B., D'Allura, A., Wei, C., and

804 Carmichael, G. R.: Source sector and region contributions to BC and $PM_{2.5}$ in Central
805 Asia, Atmos. Chem. Phys., 15, 1683-1705, doi: 10.5194/acp-15-1683-2015, 2015.

806 Kumar, B., Chakraborty, A., Tripathi, S. N., and Bhattu, D.: Highly time resolved chemical
807 characterization of submicron organic aerosols at a polluted urban location,
808 Environmental Science: Processes & Impacts, 18, 1285-1296, 10.1039/C6EM00392C,
809 2016a.

810 Kumar, M., Tiwari, S., Murari, V., Singh, A. K., and Banerjee, T.: Wintertime characteristics of
811 aerosols at middle Indo-Gangetic Plain: Impacts of regional meteorology and long range
812 transport, Atmospheric Environment, 104, 162-175, 10.1016/j.atmosenv.2015.01.014,
813 2015.

814 Kumar, V., Sarkar, C., and Sinha, V.: Influence of post harvest crop residue fires on surface
815 ozone mixing ratios in the NW IGP analyzed using two years of continuous in-situ trace
816 gas measurements, J. Geophys. Res. Atmos., 121, 3619–3633, doi:
817 10.1002/2015JD024308, 2016b.

818 Lawrence, M. G., and Lelieveld, J.: Atmospheric pollutant outflow from southern Asia: a review,
819 Atmos. Chem. Phys., 10, 11017-11096, doi: 10.5194/acp-10-11017-2010, 2010.

820 Lüthi, Z. L., Škerlak, B., Kim, S. W., Lauer, A., Mues, A., Rupakheti, M., and Kang, S.:
821 Atmospheric brown clouds reach the Tibetan Plateau by crossing the Himalayas,
822 Atmospheric Chemistry and Physics, 15, 6007-6021, 10.5194/acp-15-6007-2015, 2015.

823 Marinoni, A., Cristofanelli, P., Laj, P., Duchi, R., Putero, D., Calzolari, F., Landi, T. C.,
824 Vuillermoz, E., Maione, M., and Bonasoni, P.: High black carbon and ozone
825 concentrations during pollution transport in the Himalayas: Five years of continuous
826 observations at NCO-P global GAW station, Journal of environmental Science, 25, 1618-
827 1625, doi: 10.1016/s1001-0742(12)60242-3, 2013.

828 Misra, A., Gaur, A., Bhattu, D., Ghosh, S., Dwivedi, A. K., Dalai, R., Paul, D., Gupta, T., Tare,
829 V., Mishra, S. K., Singh, S., and Tripathi, S. N.: An overview of the physico-chemical
830 characteristics of dust at Kanpur in the central Indo-Gangetic basin, Atmospheric
831 Environment, 97, 386-396, http://dx.doi.org/10.1016/j.atmosenv.2014.08.043, 2014.

832 Mohnen, V. A., Goldstein, W., and Wang, W. C.: Tropospheric Ozone and Climate Change, Air
833 & Waste, 43, 1332-1334, 10.1080/1073161x.1993.10467207, 1993.

834 Naja, M., Lal, S., and Chand, D.: Diurnal and seasonal variabilities in surface ozone at a high
835 altitude site Mt Abu (24.6^0 N, 72.7^0 E, 1680m asl) in India, Atmospheric Environment,
836 37, 4205-4215, doi: 10.1016/S1352-2310(03)00565-X, 2003.

837 Pan, X. L., Kanaya, Y., Wang, Z. F., Liu, Y., Pochanart, P., Akimoto, H., Sun, Y. L., Dong, H.
838 B., Li, J., Irie, H., and Takigawa, M.: Correlation of black carbon aerosol and carbon
839 monoxide in the high-altitude environment of Mt. Huang in Eastern China, Atmos.
840 Chem. Phys., 11, 9735-9747, doi: 10.5194/acp-11-9735-2011, 2011.

841 Panday, A. K., and Prinn, R. G.: Diurnal cycle of air pollution in the Kathmandu Valley, Nepal:
842 Observations, Journal of Geophysical Research, 114, 1-19, doi: 10.1029/2008jd009777,
843 2009.

844 Pathak, B., Bhuyan, P. K., Biswas, J., and Takemura, T.: Long term climatology of particulate
845 matter and associated microphysical and optical properties over Dibrugarh, North-East
846 India and inter-comparison with SPRINTARS simulations, Atmospheric Environment,
847 69, 334-344, 10.1016/j.atmosenv.2012.12.032, 2013.

848 Praveen, P. S., Ahmed, T., Kar, A., Rehman, I. H., and Ramanathan, V.: Link between local
849 scale BC emissions in the Indo-Gangetic Plains and large scale atmospheric solar
850 absorption, Atmospheric Chemistry and Physics, 12, 1173-1187, 10.5194/acp-12-1173-
851 2012, 2012.

852 Putero, D., Landi, T., Cristofanelli, P., Marinoni, A., Laj, P., Duchi, R., Calzolari, F., Verza, G.,
853 and Bonasoni, P.: Influence of open vegetation fires on black carbon and ozone
854 variability in the southern Himalayas (NCO-P, 5079 m asl), Environmental Pollution,
855 184, 597-604, 10.1016/j.envpol.2013.09.035, 2014.

856 Putero, D., Cristofanelli, P., Marinoni, A., Adhikary, B., Duchi, R., Shrestha, S. D., Verza, G. P.,
857 Landi, T. C., Calzolari, F., Busetto, M., Agrillo, G., Biancofiore, F., Di Carlo, P., Panday,
858 A. K., Rupakheti, M., and Bonasoni, P.: Seasonal variation of ozone and black carbon
859 observed at Paknajol, an urban site in the Kathmandu Valley, Nepal, Atmospheric
860 Chemistry and Physics, 15, 13957-13971, 10.5194/acp-15-13957-2015, 2015.

861 Ram, K., Sarin, M., and Tripathi, S.: A 1 year record of carbonaceous aerosols from an urban site
862 in the Indo-Gangetic Plain: Characterization, sources, and temporal variability, J.
863 Geophys. Res., 115, D24313, doi: 10.1029/2010JD014188, 2010.

864 Ramachandran, S., and Rajesh, T. A.: Black carbon aerosol mass concentrations over
865 Ahmedabad, an urban location in western India: Comparison with urban sites in Asia,
866 Europe, Canada, and the United States, Journal of Geophysical Research, 112, 1-19,
867 10.1029/2006JD007488, 2007.

868 Ramanathan, V., Li, F., Ramana, M., Praveen, P., Kim, D., Corrigan, C., Nguyen, H., Stone, E.
869 A., Schauer, J. J., and Carmichael, G.: Atmospheric brown clouds: Hemispherical and
870 regional variations in long-range transport, absorption, and radiative forcing, Journal of
871 Geophysical Research, 112, 1-26, 10.1029/2006JD008124, 2007.

872 Ramanathan, V., and Carmichael, G.: Global and regional climate changes due to black carbon,
873 Nature geoscience, 1, 221-227, 2008.

874 Rastogi, N., Singh, A., Sarin, M. M., and Singh, D.: Temporal variability of primary and
875 secondary aerosols over northern India: Impact of biomass burning emissions, Atmos.
876 Environ., 125, 396-403, doi: 10.1016/j.atmosenv.2015.06.010, 2016.

877 Rehman, I. H., Ahmed, T., Praveen, P. S., Kar, A., and Ramanathan, V.: Black carbon emissions
878 from biomass and fossil fuels in rural India, Atmospheric Chemistry and Physics, 11,
879 7289-7299, 10.5194/acp-11-7289-2011, 2011.

880 Safai, P. D., Kewat, S., Pandithurai, G., Praveen, P. S., Ali, K., Tiwari, S., Rao, P. S. P.,
881 Budhawant, K. B., Saha, S. K., and Devara, P. C. S.: Aerosol characteristics during
882 winter fog at Agra, North India, J. Atmos. Chem., 61, 101-118, doi: 10.1007/s10874-009-
883 9127-4, 2009.

884 Sandradewi, J., Prévôt, A. S. H., Szidat, S., Perron, N., Alfarra, M. R., Lanz, V. A., Weingartner,
885 E., and Baltensperger, U.: Using Aerosol Light Absorption Measurements for the
886 Quantitative Determination of Wood Burning and Traffic Emission Contributions to
887 Particulate Matter, Environmental Science & Technology, 42, 3316-3323, doi:
888 10.1021/es702253m, 2008.

889 Sarkar, C., Kumar, V., and Sinha, V.: Massive emissions of carcinogenic benzenoids from paddy
890 residue burning in north India, Curr. Sci. India, 104, 1703-1709, 2013.

891 Schmid, O., Artaxo, P., Arnott, W. P., Chand, D., Gatti, L. V., Frank, G. P., Hoffer, A.,
892 Schnaiter, M., and Andreae, M. O.: Spectral light absorption by ambient aerosols
893 influenced by biomass burning in the Amazon Basin. I: Comparison and field calibration
894 of absorption measurement techniques, Atmospheric Chemistry and Physics, 6, 3443-
895 3462, doi: 10.5194/acp-6-3443-2006, 2006.

896 Sharma, R. K., Bhattarai, B. K., Sapkota, B. K., Gewali, M. B., and Kjeldstad, B.: Black carbon
897 aerosols variation in Kathmandu valley, Nepal, Atmos. Environ., 63, 282-288,
898 10.1016/j.atmosenv.2012.09.023, 2012.

899 Sharma, S., Brook, J. R., Cachier, H., Chow, J., Gaudenzi, A., and Lu, G.: Light absorption and
900 thermal measurements of black carbon in different regions of Canada, Journal of
901 Geophysical Research: Atmospheres, 107 (D24), 1-11, 10.1029/2002JD002496, 2002.

902 Shindell, D., Kuylenstierna, J. C., Vignati, E., van Dingenen, R., Amann, M., Klimont, Z.,
903 Anenberg, S. C., Muller, N., Janssens-Maenhout, G., and Raes, F.: Simultaneously
904 mitigating near-term climate change and improving human health and food security,
905 Science, 335, 183-189, 2012.

906 Singh, N., Murari, V., Kumar, M., Barman, S. C., and Banerjee, T.: Fine particulates over South
907 Asia: Review and meta-analysis of PM2.5 source apportionment through receptor model,
908 Environmental Pollution, 223, 121-136, 10.1016/j.envpol.2016.12.071, 2017.

909 Sinha, V., Kumar, V., and Sarkar, C.: Chemical composition of pre-monsoon air in the Indo-
910 Gangetic Plain measured using a new air quality facility and PTR-MS: high surface
911 ozone and strong influence of biomass burning, Atmospheric Chemistry and Physics, 14,
912 5921-5941, 10.5194/acp-14-5921-2014, 2014.

Skamarock, W., Klemp, J., Dudhia, J., Gill, D., and Barker, D.: A description of the Advanced Research WRF version 3,Technical Report NCAR/TN475+STR, National Center for Atmospheric Research Technical Note, Boulder, Colorado, 2008.

Snider, G., Weagle, C. L., Murdymootoo, K. K., Ring, A., Ritchie, Y., Stone, E., Walsh, A., Akoshile, C., Anh, N. X., Balasubramanian, R., Brook, J., Qonitan, F. D., Dong, J., Griffith, D., He, K., Holben, B. N., Kahn, R., Lagrosas, N., Lestari, P., Ma, Z., Misra, A., Norford, L. K., Quel, E. J., Salam, A., Schichtel, B., Segev, L., Tripathi, S., Wang, C., Yu, C., Zhang, Q., Zhang, Y., Brauer, M., Cohen, A., Gibson, M. D., Liu, Y., Martins, J. V., Rudich, Y., and Martin, R. V.: Variation in global chemical composition of PM2.5: emerging results from SPARTAN, Atmospheric Chemistry and Physics, 16, 9629-9653, 10.5194/acp-16-9629-2016, 2016.

Stevenson, D., Dentener, F., Schultz, M., Ellingsen, K., Van Noije, T., Wild, O., Zeng, G., Amann, M., Atherton, C., and Bell, N.: Multimodel ensemble simulations of present-day and near-future tropospheric ozone, Journal of Geophysical Research, 111, D08301, 1-23, 10.1029/2005JD006338, 2006.

Tiwari, S., Srivastava, A. K., Bisht, D. S., Parmita, P., Srivastava, M. K., and Attri, S. D.: Diurnal and seasonal variations of black carbon and PM2.5 over New Delhi, India: Influence of meteorology, Atmospheric Research, 125-126, 50-62, 10.1016/j.atmosres.2013.01.011, 2013.

Tiwari, S., Pipal, A. S., Hopke, P. K., Bisht, D. S., Srivastava, A. K., Tiwari, S., Saxena, P. N., Khan, A. H., and Pervez, S.: Study of the carbonaceous aerosol and morphological analysis of fine particles along with their mixing state in Delhi, India: a case study, Environmental Science and Pollution Research, 22, 10744-10757, 10.1007/s11356-015-4272-6, 2015.

Tiwari, S., Dumka, U. C., Kaskaoutis, D. G., Ram, K., Panicker, A. S., Srivastava, M. K., Tiwari, S., Attri, S. D., Soni, V. K., and Pandey, A. K.: Aerosol chemical characterization and role of carbonaceous aerosol on radiative effect over Varanasi in central Indo-Gangetic Plain, Atmospheric Environment, 125, 437-449, 10.1016/j.atmosenv.2015.07.031, 2016.

Tiwari, S., Dumka, U. C., Gautam, A. S., Kaskaoutis, D. G., Srivastava, A. K., Bisht, D. S., Chakrabarty, R. K., Sumlin, B. J., and Solmon, F.: Assessment of $PM_{2.5}$ and PM_{10} over Guwahati in Brahmaputra River Valley: Temporal evolution, source apportionment and meteorological dependence, Atmospheric Pollution Research, 8, 13-28, 10.1016/j.apr.2016.07.008, 2017.

Verma, R. L., Sahu, L. K., Kondo, Y., Takegawa, N., Han, S., Jung, J. S., Kim, Y. J., Fan, S., Sugimoto, N., Shammaa, M. H., Zhang, Y. H., and Zhao, Y.: Temporal variations of black carbon in Guangzhou, China, in summer 2006, Atmos. Chem. Phys., 10, 6471-6485, doi: 10.5194/acp-10-6471-2010, 2010.

Wan, X., Kang, S., Li, Q., Rupakheti, D., Zhang, Q., Guo, J., Chen, P., Tripathee, L., Rupakheti, M., Panday, A. K., Wang, W., Kawamura, K., Gao, S., Wu, G., and Cong, Z.: Organic molecular tracers in the atmospheric aerosols from Lumbini, Nepal, in the northern Indo-Gangetic Plain: Influence of biomass burning, Atmos. Chem. Phys. Discuss., 2017, 1-40, 10.5194/acp-2016-1176, 2017.

WHO: Air quality guidelines: global update 2005: particulate matter, ozone, nitrogen dioxide, and sulfur dioxide, World Health Organization, Geneva, 22 pp., 2006.

Wiedinmyer, C., Akagi, S. K., Yokelson, R. J., Emmons, L. K., Al-Saadi, J. A., Orlando, J. J., and Soja, A. J.: The Fire INventory from NCAR (FINN): a high resolution global model to estimate the emissions from open burning, Geosci. Model Dev., 4, 625-641, doi: 10.5194/gmd-4-625-2011, 2011.

Zhou, X., Gao, J., Wang, T., Wu, W., and Wang, W.: Measurement of black carbon aerosols near two Chinese megacities and the implications for improving emission inventories, Atmospheric Environment, 43, 3918-3924, 10.1016/j.atmosenv.2009.04.062, 2009.

966 **Table 1**. Summary of instruments deployed during monitoring in Lumbini

Instrument (Model)	Manufacturer	Parameters	Inlet/sensor height (above ground)	Sampling interval	Sampled period
Environmental Dust monitor (EDM 164)	GRIMM Aerosol Technik, Germany	PM_1, $PM_{2.5}$, PM_{10}	5 m	5 min	04/02-05/10, 06/02-06/13
Aethalometer (AE42)	Magee Scientific, USA	Aerosol light absorption at seven wavelengths, and BC concentration	3 m	5 min	01/04-05/06
CO analyzer (48*i*)	Thermo Scientific, USA	CO concentration	3 m	1 min	01/04-15/06
O_3 analyzer (49*i*)	Thermo Scientific, USA	O_3 concentration	3 m	1 min	01/04-15/06
Automatic Weather Station (AWS)	Campbell Scientific, UK	T, RH, WS, WD, Global Radiation, Precipitation	12 m	1 min	01/04-15/06

967

968

969 **Table 2.** Comparison of $PM_{2.5}$, BC, CO and O_3 concentrations at Lumbini with those at other sites in South Asia

Sites	Characteristics	Measurement period	$PM_{2.5}$ (μg m^{-3})	BC (μg/m^3)	CO (ppbv)	O_3 (ppbv)	References
Lumbini, Nepal	Semi-urban	Pre-monsoon, 2013	53.1±35.1	4.9±3.8	344.1±160.3	46.6±20.3	This study
Kathmandu, Nepal	Urban	Pre-monsoon, 2013	-	14.5±10	-	38.0±25.6	(Putero et al., 2015)
Mt. Everest, Nepal	Remote	Pre-monsoon	-	0.4±0.4	-	61.3±7.7	(Marinoni et al., 2013)
Delhi, India	Urban	Pre-monsoon (night-time)	82.3±50.5	7.70±7.25	1800±890	-	(Bisht et al., 2015)
Kanpur, India	Urban	June 2009-May 2013, April-June	-	2.1±0.9	721±403	27.9±17.8	(Gaur et al., 2014) (Ram et al., 2010)
Mohali, India	Semi-urban	May, 2012	104±80.3	-	566.7±239.2	57.8±25.4	(Sinha et al., 2014)
Mt. Abu, India	Remote	Jan 1993-Dec 2000, pre-monsoon	-	0.7±0.14	131±36	39.9±10.8	(Naja et al., 2003) (Das and Jayaraman, 2011)

970 **Table 3**. Inter-comparison of observed and model simulated hourly average concentrations of air
971 pollutants during the measurement campaign period. Unit: BC and PM in μg/m^3 and CO in ppbv.

Pollutants	Observed (mean and range)	Modeled (mean and range)	Ratio of mean (observed/modeled)
BC	4.9 (0.3-29.9)	1.8 (0.4-3.7)	2.7
PM_1	36.6 (3.6-197.6)	12.3 (0.9-41.7)	3
$PM_{2.5}$	53.1 (6.1-272.2)	17.3 (1.9-48.3)	3
PM_{10}	128.8 (10.5-604.0)	25.4 (2.1-68.8)	5
CO	344.1(124.9-1429.7)	255.7 (72.2-613.1)	1.35

972

973

Figures

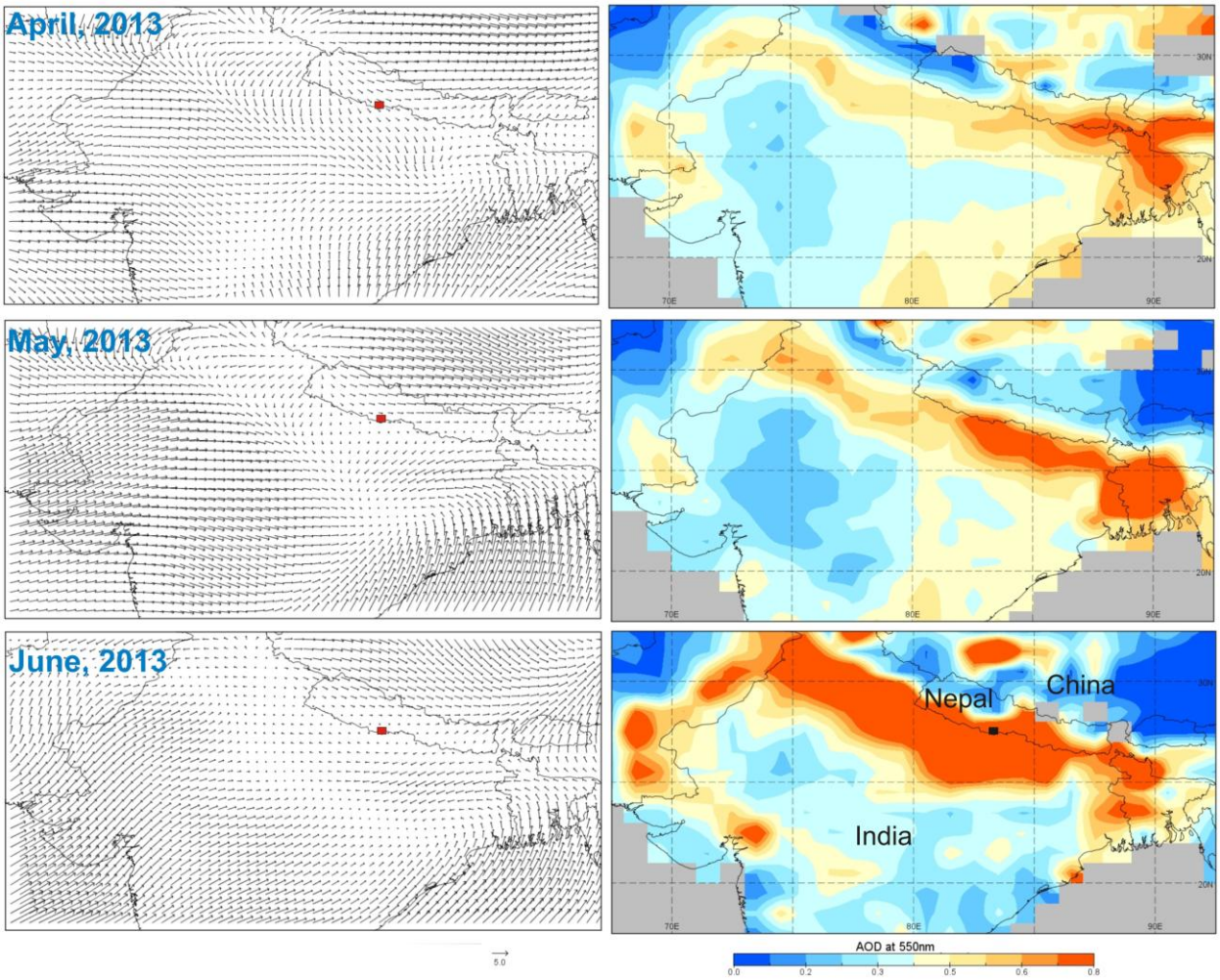

Figure 1. Monthly synoptic wind (at 1000 hPa) for April, May and June 2013, based on NCEP/NCAR reanalysis data where the orientations of arrows refer to wind direction and the length of arrows represents the magnitude of wind (m/s). Red square box in the figure (left) represents the location of Lumbini. Figures on the right side represent monthly aerosol optical depth acquired with the MODIS instrument aboard TERRA satellite. High aerosol loading can be seen over the entire Indo-Gangetic Plain (IGP). Light gray color used in the figure represents the absence of data.

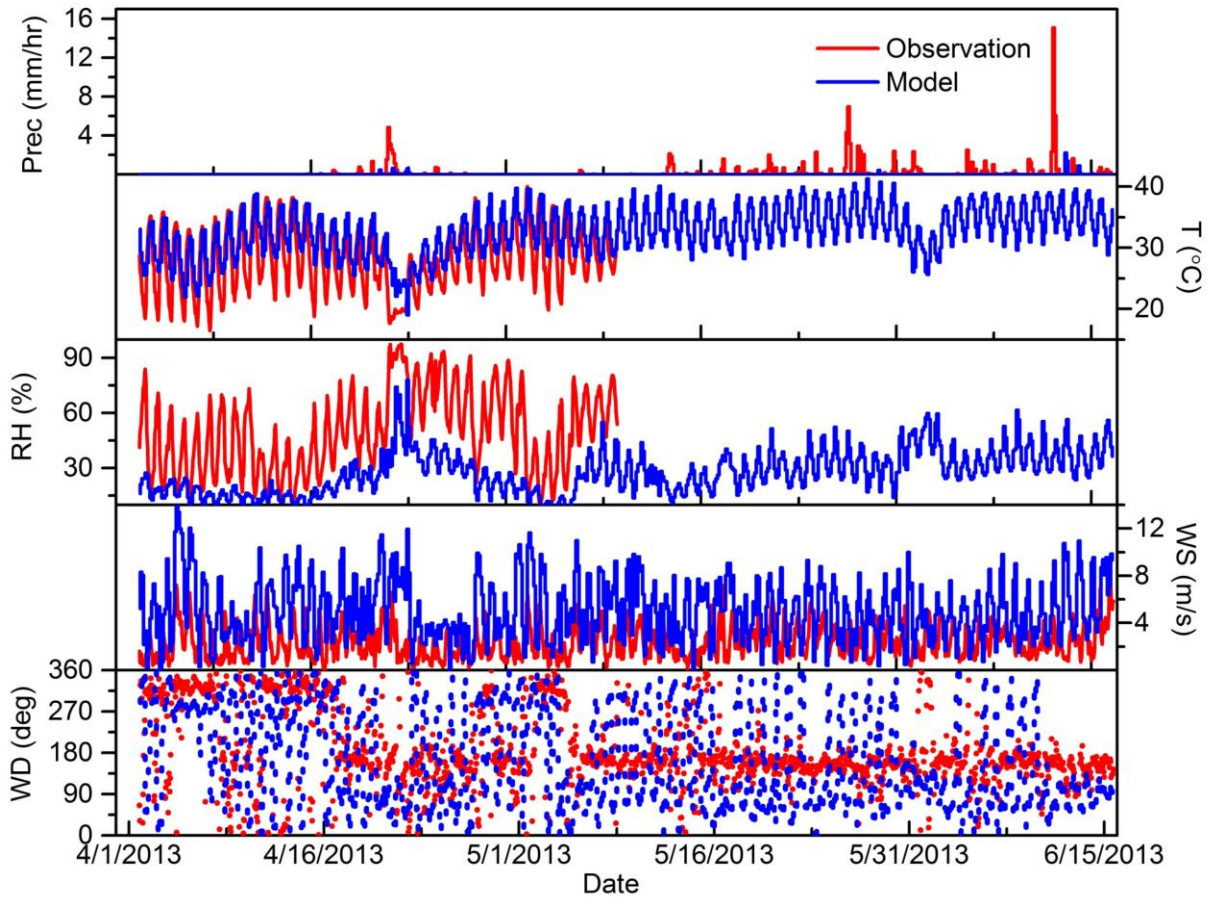

Figure 2. Time series of hourly average observed (red) and model estimated (blue) meteorological parameters at Lumbini, Nepal for the entire sampling period from 1 April to 15 June 2013.

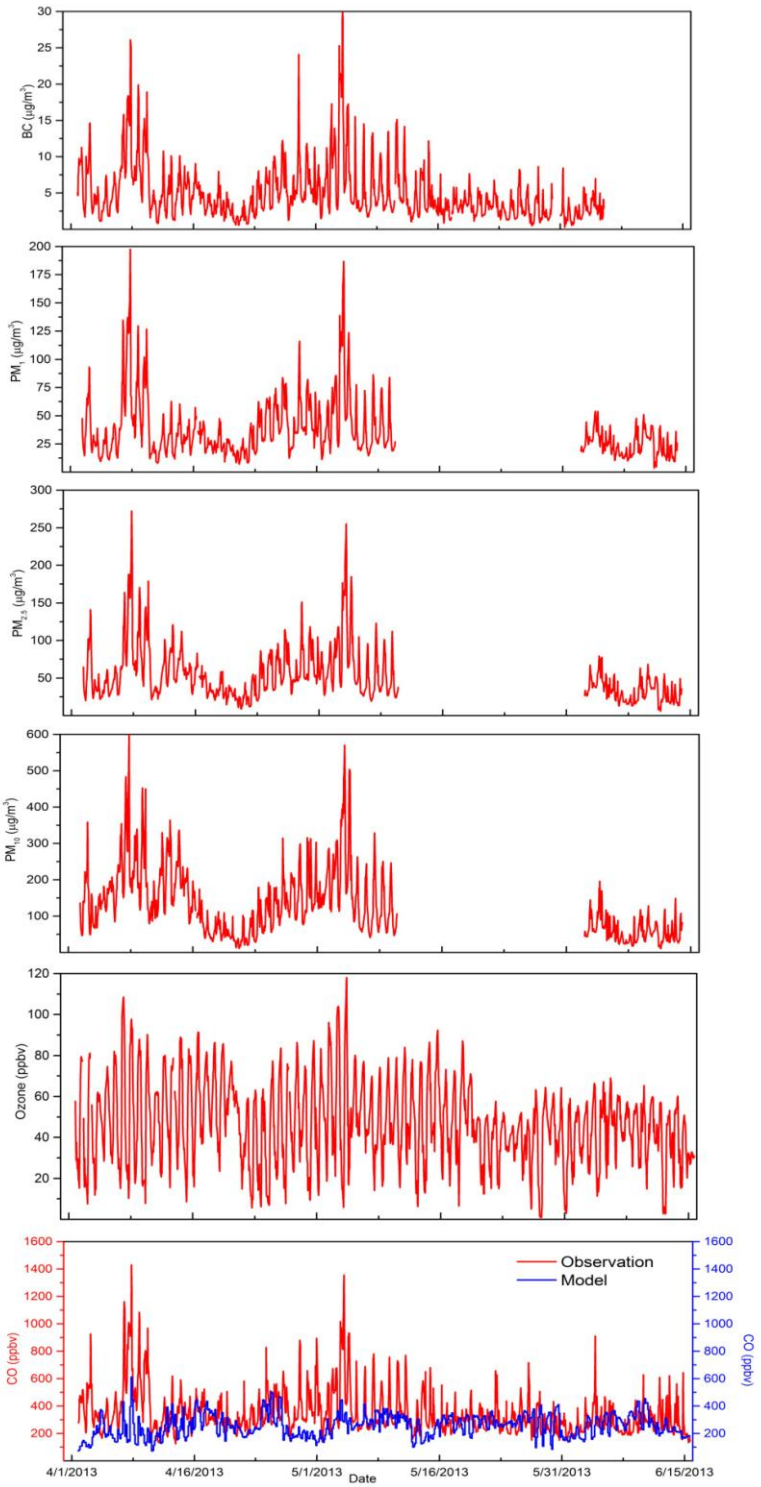

Figure 3. Time series of the observed (red line) and model estimated (blue line) hourly average concentrations of BC, PM_1, $PM_{2.5}$, PM_{10}, O_3 and CO at Lumbini, Nepal for the entire sampling period from 1 April to 15 June 2013.

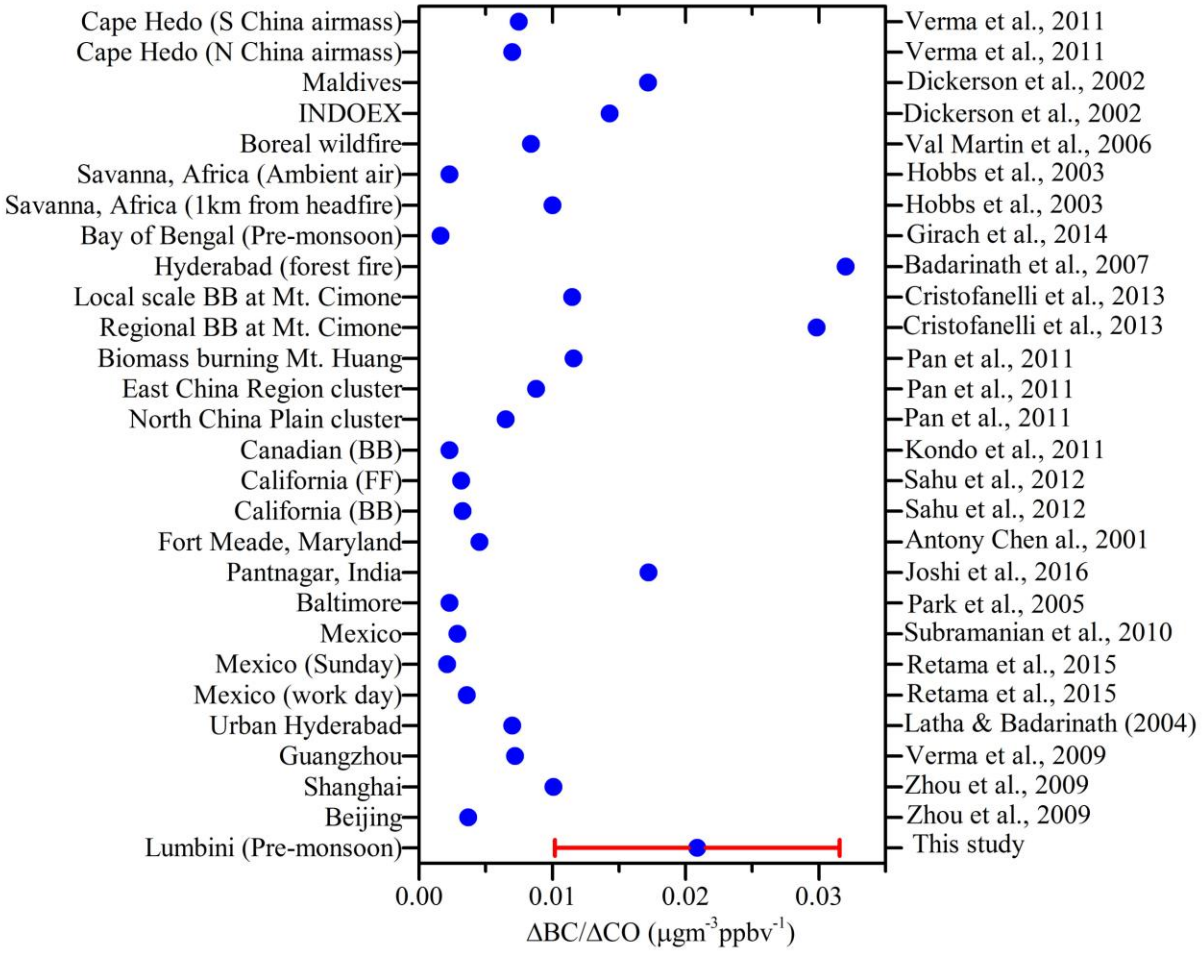

Figure 4. Comparison of BC concentrations to CO concentrations (ΔBC/ΔCO) ratios obtained for Lumbini with other sites. The red horizontal bar represents standard deviation.

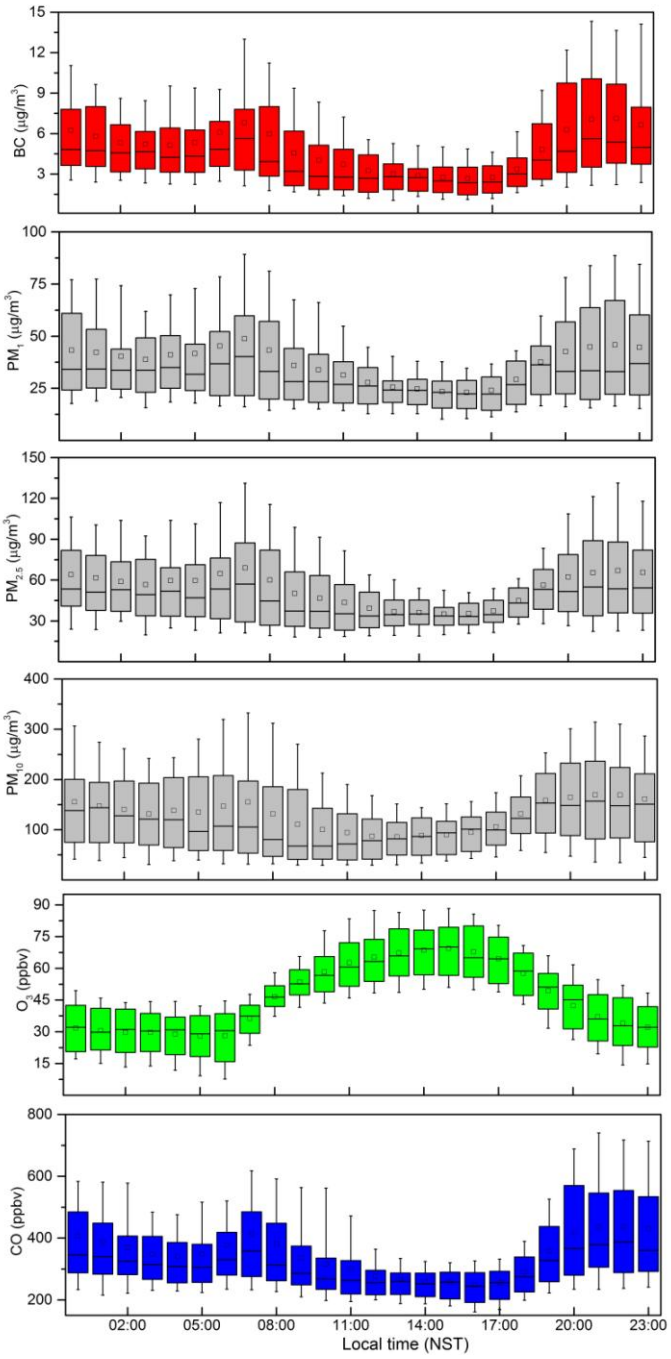

998

999 **Figure 5.** Diurnal variations of hourly average ambient concentrations of BC, PM_1, $PM_{2.5}$, PM_{10},
1000 O_3 and CO at Lumbini during the monitoring period (1 April -15 June 2013). In each box, lower
1001 and upper boundary of the box represents 25th and 75th percentile respectively, top and bottom of
1002 the whisker represents 90th and 10th percentile respectively, the mid-line represents median, and
1003 the square mark represents the mean for each hour.

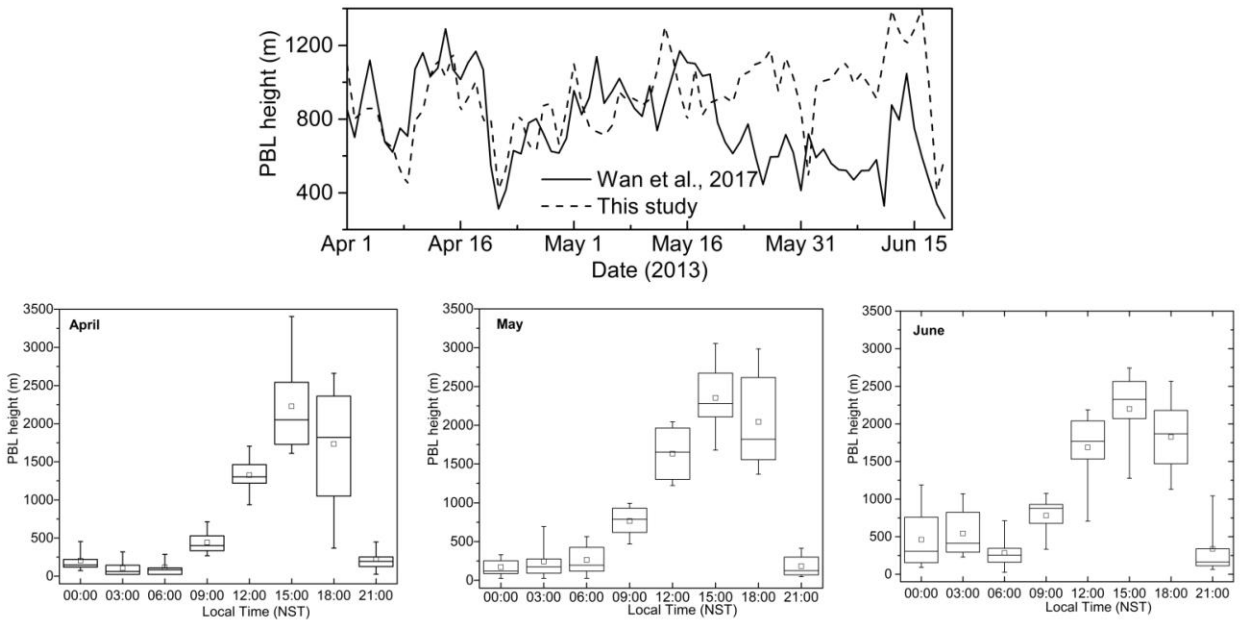

1004

1005 **Figure 6.** Daily time series of PBL height obtained from the model and reported values over
1006 Lumbini (obtained from Xin et al., 2017). The lower panel shows the monthly average diurnal
1007 variation of the PBL height. The square mark in each box represents the mean PBL height,
1008 bottom and top of the box represents 25^{th} and 75^{th} percentile, top and bottom of the whisker
1009 represents 90^{th} and 10^{th} percentile respectively.

1010

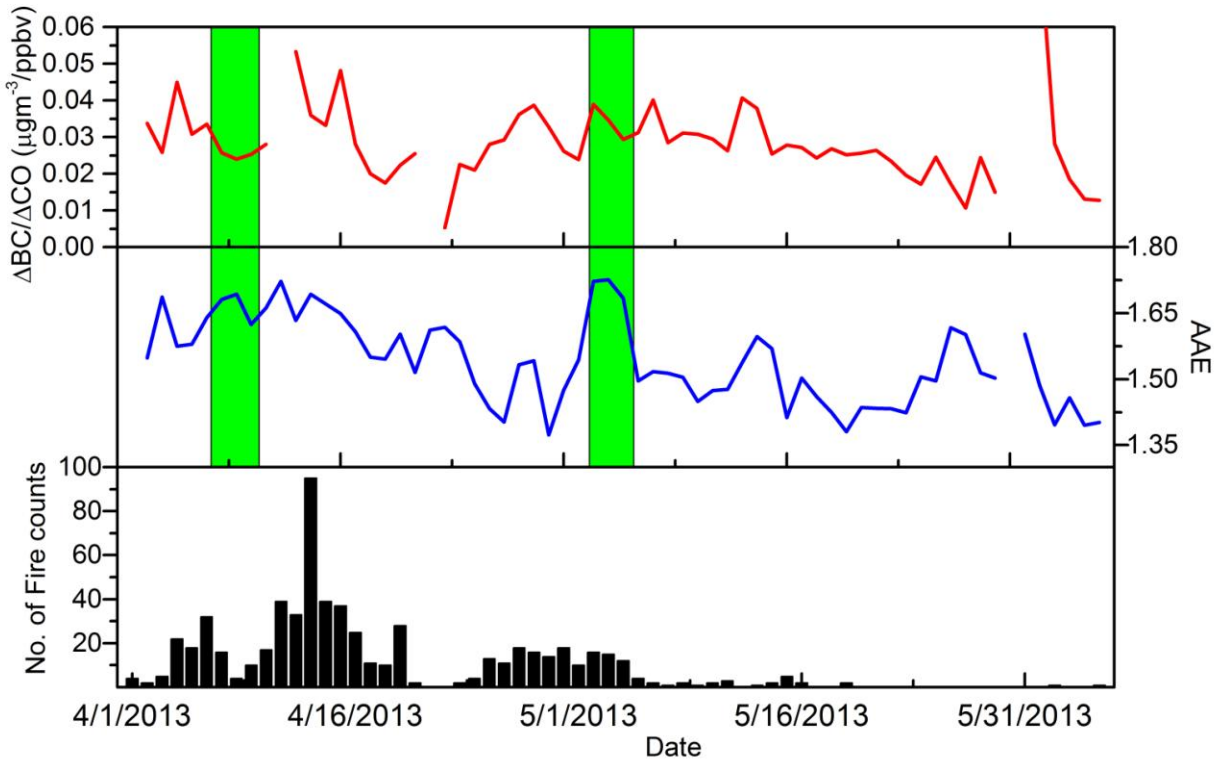

Figure 7. Time series of daily average ΔBC/ΔCO ratio, absorption Ångstrom exponent (AAE), along with fire counts acquired with the MODIS instrument onboard TERRA satellite for a 200×200 km grid centered at Lumbini. Two rectangular green boxes represent time of two episodes with high peaks in CO and BC concentrations as shown in Fig. 3.

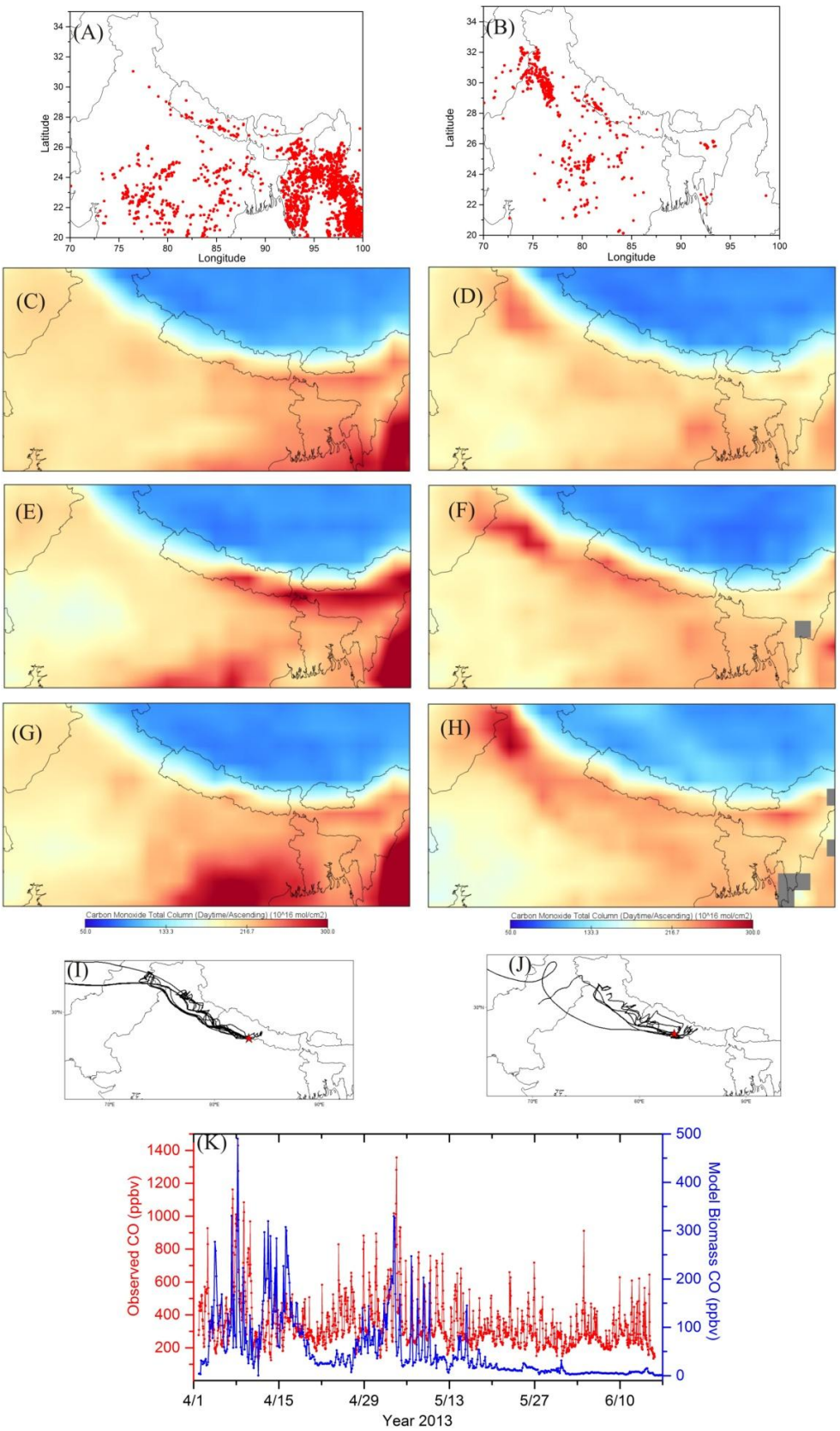
(A)
(B)
Latitude
Longitude
(C)
(D)
(E)
(F)
(G)
(H)
Carbon Monoxide Total Column (Daytime/Ascending) (10^16 mol/cm2)
(I)
(J)
(K)
Observed CO (ppbv)
Model Biomass CO (ppbv)
Year 2013
4/1
4/15
4/29
5/13
5/27
6/10

1017

Figure 8. Active fire hotspots in the region acquired with the MODIS instrument on Aqua satellite during (A) Event-I (7-9 April) and (B) Event-II (3-4 May). CO emissions, acquired with AIRS satellite, in the region two days before (3-5 April), during (7-9 April) and two days after (10-12 April) the Event-I are shown in panels (C), (E) and (G), respectively while panels (D), (F) and (H) show CO emissions two days before (1-2 May), during (3-4 May) and two days after (5-6 May) the Event-II. Panels (I) and (J) represent the 6-hr interval HYSPLIT back trajectories during Event I and II, respectively. Location of the Lumbini site is indicated by the red star in the panel (I and J). Observed CO versus Model open burning CO illustrating the contribution of forest fires during peak CO loading is shown in panel (K).

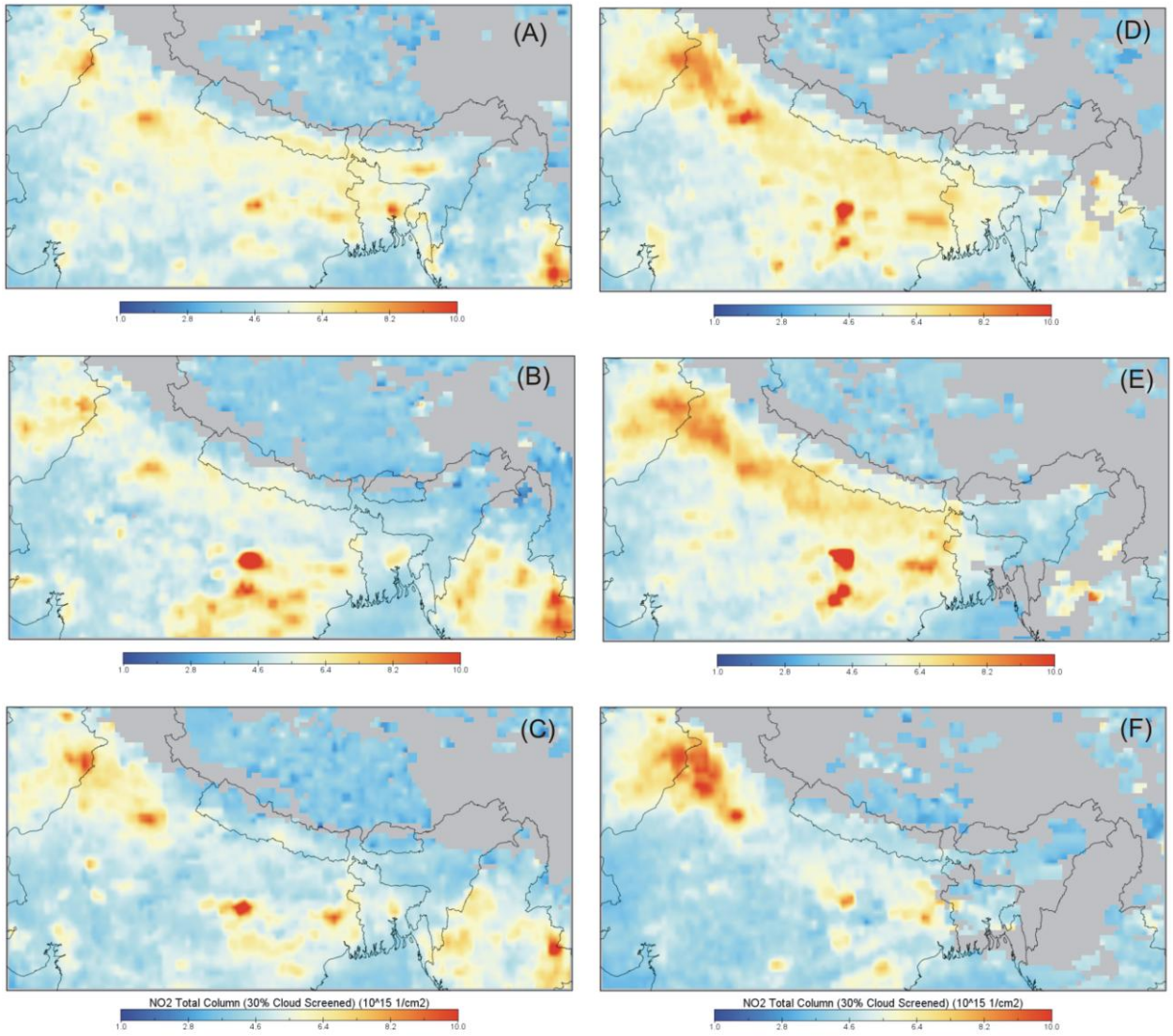

Figure 9. NO_2 total column obtained with OMI satellite over the region (A) before, (B) during, and (C) after the Event- I. The panels (D), (E), (F) show NO_2 total column before, during and after the Event- II.

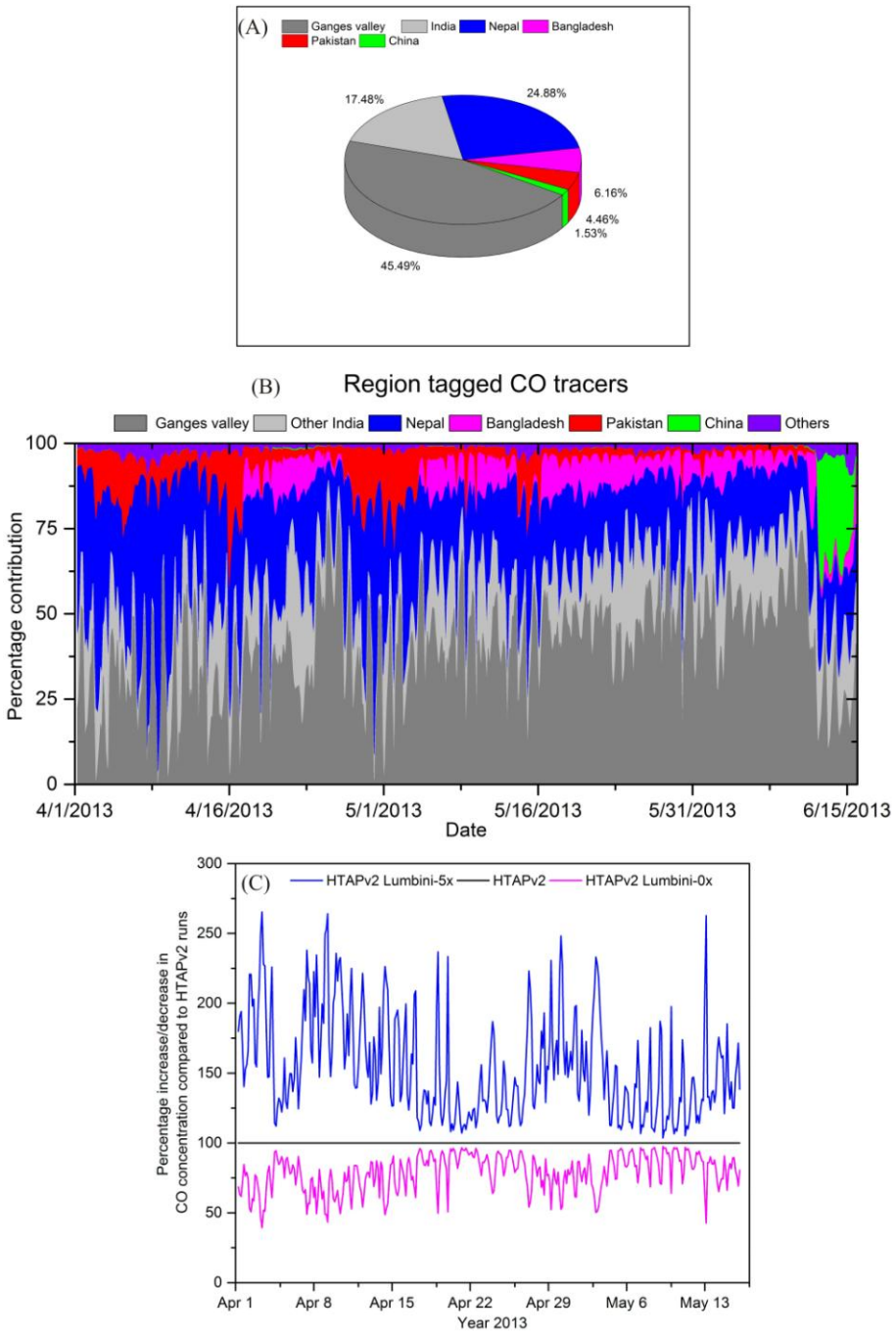

1034

1035 **Figure 10.** (A) WRF-STEM model estimated contributions of various source regions to average
1036 CO concentration in Lumbini for the sampling period, (B) time series of region tagged CO tracer
1037 during the whole measurement period using HTAP emission inventory and (C) Figure showing
1038 percentage increase/decrease in CO concentration with different emissions scenario.

1039

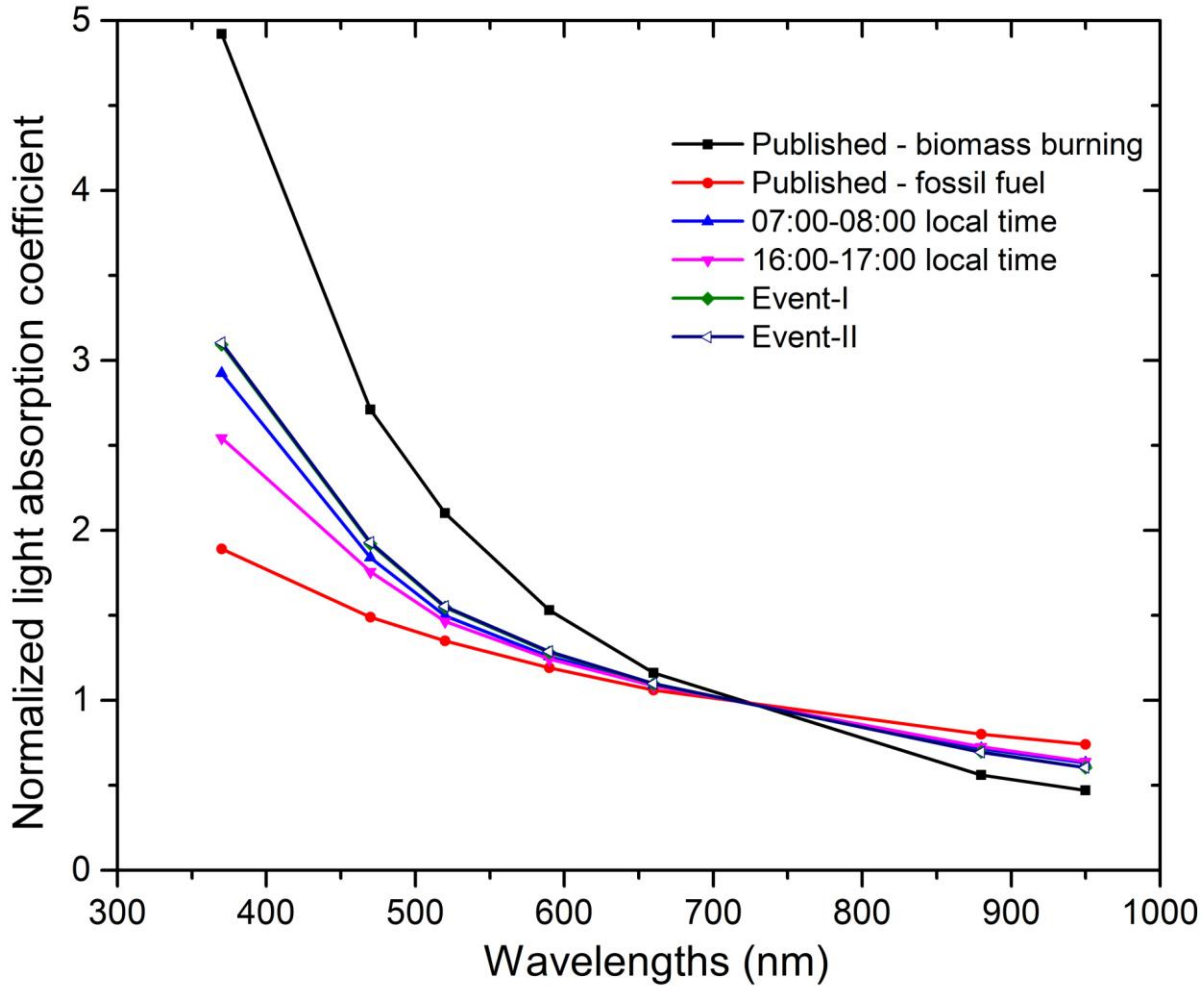

1040

1041 **Figure 11.** Comparison of normalized spectral light absorption coefficients obtained during the
1042 prime cooking (07:00-08:00 local time) and non cooking time (16:00-17:00 LT) at Lumbini with
1043 published data from Kirchstetter et al. (2004).

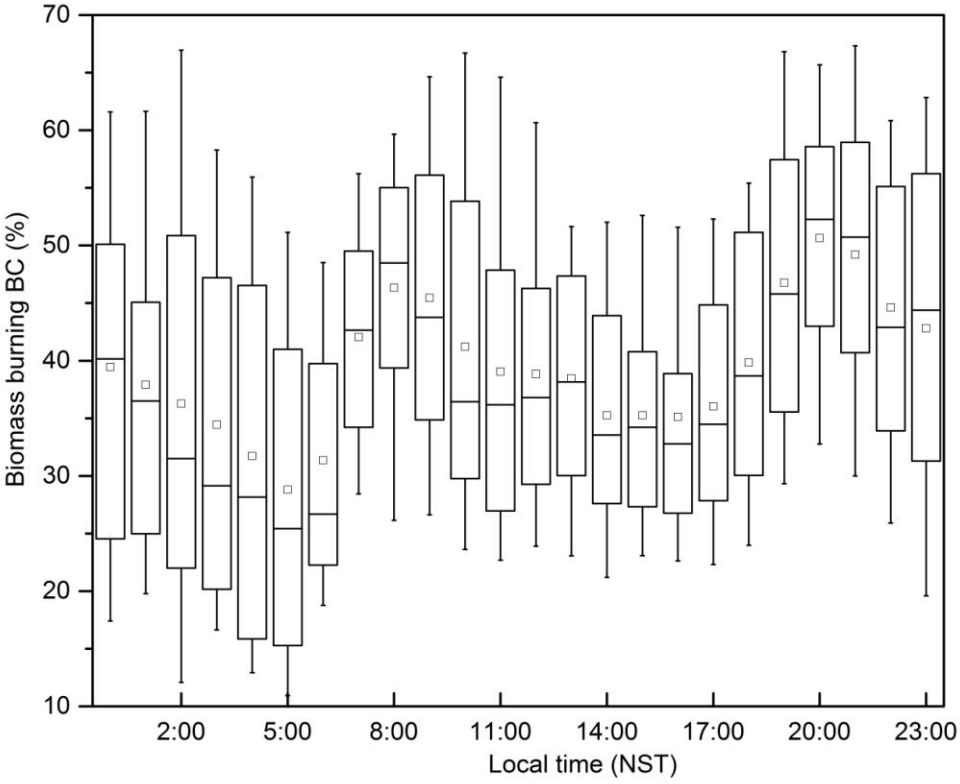

Figure 12. Diurnal variation of the fractional contribution of biomass burning to ambient BC concentration at Lumbini for the measurement period. In each box, lower and upper boundary of the box represent 25th and 75th percentile, respectively, top and bottom of the whisker represents 90th and 10th percentile, respectively. The mid-line in each box represents median while the square mark represents the mean for each hour.